Meiotic DSB-independent role of protein phosphatase 4 in Hop1 assembly to promote meiotic chromosome axis formation in budding yeast

Ke Li[1,2], Miki Shinohara[1,3,4,*]

[1]Institute for Protein Research, Osaka University, Suita, Osaka 565-0871, Japan

[2]Department of Bioscience, Graduate School of Science, Osaka University, Toyonaka, Osaka 560-0043, Japan

[3]Department of Advanced Bioscience, Graduate School of Agriculture, Kindai University, Nara city, Nara 631-8505, Japan

[4]Agricultural Technology and Innovation Research Institute, Kindai University, Nara city, Nara 631-8505, Japan

∗Correspondence:

Miki Shinohara

Department of Advanced Bioscience, Graduate School of Agriculture, Kindai University

3327-204 Nakamachi, Nara, Nara city 631-8505, Japan

Phone: +81-742-43-6518

FAX: +81-742-43-8976

E-mail: mikis@nara.kindai.ac.jp

ORCID ID: 0000-0002-7413-8235

Running title: Novel function of PP4 in Hop1 assembly

Abstract

Dynamic changes in chromosomal structure that occur during meiotic prophase play an important role in the progression of meiosis. Among these structures, meiosis-specific chromosomal axis-loop structures are important as a scaffold for integrated control between the meiotic recombination reaction and the associated checkpoint system to ensure accurate chromosome segregation. However, the molecular mechanism of the initial step of chromosome axis-loop construction is not well understood. Here, we showed that in budding yeast, protein phosphatase 4 (PP4) that primarily counteracts Mec1/Tel1 phosphorylation is required to promote the assembly of chromosomal axis components Hop1 and Red1 onto meiotic chromatin via interaction with Hop1. PP4, in contrast, did not affect Rec8 assembly. Notably, unlike the previously known function of PP4, this novel function of PP4 was independent of meiotic DSB-dependent Tel1/Mec1 kinase activities. The defect in Hop1/Red1 assembly in the absence of PP4 function was not suppressed by dysfunction of Pch2, which removes Hop1 protein from the chromosome axis. This suggests that PP4 is required for the initial step of chromatin loading of Hop1 rather than stabilization of Hop1 on axes. These results indicate that phosphorylation/dephosphorylation-mediated regulation of Hop1 recruitment onto chromatin occurs during chromosome axis construction before meiotic double-strand break formation. (199 words)

Introduction

Meiotic recombination is essential for proper segregation of homologous chromosomes during the first meiotic division (meiosis-I). This process is initiated by Spo11-dependent programmed meiotic DNA double-strand break (DSB) formation at meiotic recombination hot spots (KEENEY 2001). Meiotic DSB formation and subsequent meiotic recombination require the specific scaffold of an axis-loop structure of chromatin (SHINOHARA *et al.* 2000; BLAT *et al.* 2002; PANIZZA *et al.* 2011).The highly conserved meiotic chromosome axis structure contains core factors, Red1, Hop1, and meiosis-specific cohesin complexes, including the meiosis-specific subunit Rec8 in budding yeast (ROCKMILL AND ROEDER 1988; HOLLINGSWORTH AND BYERS 1989; KLEIN *et al.* 1999). After meiotic DSB formation, recombinases Rad51/Dmc1 are recruited to single-stranded DSB ends (BISHOP *et al.* 1992; BISHOP 1994; SHINOHARA *et al.* 1997). The single-stranded DSB ends promote the assembly of Zip-Msh-Mer/synapsis initiation complex (ZMM/SIC) proteins, including the transverse element component Zip1, to construct the synaptonemal complex (SC) and promote crossover (CO) formation (SYM *et al.* 1993; NOVAK *et al.* 2001; BORNER *et al.* 2004; SHINOHARA *et al.* 2008; SHINOHARA *et al.* 2015; DE MUYT *et al.* 2018). In the early leptotene, Zip1 with Zip3 localizes to the centromere and mediates centromere pairing, an initial process that ultimately promotes chromosomal pairing (TSUBOUCHI AND ROEDER 2005; FALK *et al.* 2010).

Hop1 is an axis-associated HORMA-domain protein that plays multiple roles during meiotic recombination. Hop1 is required for efficient meiotic DSB formation, inter-homolog bias in meiotic recombination, and meiotic prophase checkpoint activation and inactivation (HOLLINGSWORTH *et al.* 1990; SCHWACHA AND KLECKNER

71 1997; NIU *et al.* 2005; CARBALLO *et al.* 2008; PANIZZA *et al.* 2011; WEST *et al.* 2018).
72 Hop1 together with Red1 promotes DSB formation. Hop1 is phosphorylated by
73 Tel1/Mec1 (yeast ATM/ATR) kinases. These DSB sensor kinases activate the meiotic
74 prophase checkpoint signaling pathway via Mek1/Mre4 kinase in response to meiotic
75 recombination and synapsis defects (NIU *et al.* 2005; CARBALLO *et al.* 2008; HO AND
76 BURGESS 2011; PENEDOS *et al.* 2015; HERRUZO *et al.* 2016). Hop1, Red1, and
77 Mek1/Mre4 form the RHM complex involved in forming a stable axis structural scaffold
78 for integrating recombination, as well as the required regulatory responses associated
79 therewith. During meiotic DSB repair, homolog synapsis, mediated by SC formation,
80 and a conserved AAA+ ATPase Pch2 promote Hop1 removal from the synapsed
81 chromosome axis and attenuate the checkpoint signal (BORNER *et al.* 2008; HERRUZO
82 *et al.* 2016). Recently, Pch2 was demonstrated to be involved in the activation, as well
83 as the inactivation, of meiotic prophase checkpoints through Hop1 (RAINA AND VADER
84 2020). Thus, Hop1 phosphorylation plays a key role in completing proper meiotic
85 recombination.
86 Mec1 plays a major role in both maintaining genome integrity and meiotic
87 recombination (KATO AND OGAWA 1994; WEINERT *et al.* 1994). Mec1 is an essential
88 protein in budding yeast and *SML1* mutations can suppress the lethality of *mec1*
89 disruption (ZHAO *et al.* 1998). Tel1 and Mec1 (Tel1/Mec1) play such subtly redundant
90 roles that the *tel1 mec1* double mutant lends to a senescent phenotype (RITCHIE *et al.*
91 1999). Tel1/Mec1 is also required for integrated meiotic recombination and checkpoint
92 activation. Mec1/Tel1 kinase intra-chromosomally regulates the distribution of meiotic
93 DSB formation sites (ANDERSON *et al.* 2015; JOSHI *et al.* 2015; CHALLA *et al.* 2019). It
94 also regulates signal transduction in the meiotic DSB formative positive/negative

95 feedback loop through Rec114 phosphorylation (CARBALLO *et al.* 2013) . In addition,
96 Mec1/Tel1 mediates both DSB interference as well as CO interference, thus lending to
97 proper non-random distribution of meiotic COs (ZHANG *et al.* 2011; GARCIA *et al.* 2015;
98 SHINOHARA *et al.* 2019).

99 Protein phosphatase 4 (PP4) is a conserved putative serine/threonine protein
100 phosphatase. It functions specifically, in response to DNA damage, in attenuating the
101 phosphorylation signal of Mec1 and Tel1 during mitosis and meiosis (HOFFMANN *et al.*
102 1994; KEOGH *et al.* 2006; O'NEILL *et al.* 2007; FALK *et al.* 2010; LAI *et al.* 2011;
103 HUSTEDT *et al.* 2015). Mec1/Tel1 phosphorylates many target proteins including
104 Rad53, an ortholog of Chk2 kinase in budding yeast. In the mitotic DNA damage
105 response pathway, PP4 dephosphorylates these targets in the process of recovery
106 from DNA damage-induced signal transduction (O'NEILL *et al.* 2007). Several studies
107 have revealed the meiotic DSB-associated function of PP4 during meiotic
108 recombination (FALK *et al.* 2010; CHUANG *et al.* 2012). During meiosis, centromere
109 pairing is regulated by the balance of phosphorylation and dephosphorylation of Zip1
110 through Mec1/Tel1 kinase and PP4 phosphatase (FALK *et al.* 2010).

111 Here, we focused on the novel function of PP4, which works independently of
112 meiotic DSB formation and its associated Mec1/Tel1 activity in early prophase-I. We
113 were especially interested in the mechanics of its proper meiotic chromosome axis
114 construction via physical interaction with Hop1 protein.

115 Results

116 **PP4 activity is required for timely meiotic DSB formation and efficient CO**

117 **formation**

118 Pph3 is the catalytic subunit of the yeast PP4 complex. Pph3 contains several

119 serine/threonine phosphatase motifs (HOFFMANN *et al.* 1994). We constructed a

120 catalytic mutation in the yeast *PPH3* gene by substituting the conserved histidine

121 residue 112 required for phosphate binding with asparagine (SHI 2009), to generate the

122 *pph3-H112N* mutant (Figure 1A). It is reported that Pph3 is required for Rad53

123 dephosphorylation and DNA damage repair in mitotic cells (O'NEILL *et al.* 2007). The

124 *pph3-H112N* mutation did not affect the protein production of another PP4 subunit

125 Psy2, which was analyzed with conjugation of a 13-repeated Myc epitope tag (Psy2-

126 13Myc) (Figure S1A). In addition, we analyzed the assembly of Psy2-13Myc on meiotic

127 chromatin in pachytene cells (Figure 1B). Consistent with a previous study (FALK *et al.*

128 2010), we detected Psy2-13Myc signals as punctate foci on meiotic chromatin.

129 Importantly, the *pph3-H112N* mutation did not affect the Psy2-13Myc localization. Pph3

130 and Psy2 form a very stable PP4 complex (O'NEILL *et al.* 2007), thus suggesting that

131 the catalytic activity of PP4 is not required for its meiotic chromatin localization. Falk et

132 al. already reported the meiotic phenotypes of the *pph3*-null (*pph3*Δ) mutant (FALK *et*

133 *al.* 2010). Therefore, we characterized two *pph3* mutants, *pph3*Δ and *pph3-H112N*, to

134 better understand the function of PP4 and its phosphatase activity during meiosis.

135 First, it was revealed that both *pph3* mutants showed similarly delayed meiosis

136 progression compared to the wild type (Figure S1B). This finding was consistent with a

137 previous study on meiosis progression in the *pph3*Δ and *psy2*Δ mutants (FALK *et al.*

138 2010).

139 To confirm whether delayed meiosis progression in *pph3* mutants is caused by
140 meiotic recombination defects, we analyzed programmed meiotic DSB formation as an
141 initial event of meiotic recombination. Toward this end, Southern blotting was applied at
142 the *HIS4-LEU2* hot spot in chromosome III in the *pph3* mutants, although meiotic
143 crossover formation defects in *pph3*Δ have already been reported (FALK *et al.* 2010).
144 The *HIS4-LEU2* hot spot is a well-analyzed artificial meiotic DSB hotspot that includes
145 two known sites, DSB I and II (Figure 1C). We detected and quantified DSB I and
146 showed its frequency at each time point after meiotic entry (Figure 1D). Meiotic DSBs
147 became detectable 3 h after meiosis entry, showed a peak at 4 h, and disappeared by
148 6 h in the wild type (Figure 1D). In contrast, both *pph3-H112N* and *pph3*Δ showed an
149 approximate 1 h delay in DSB formation compared to that in the wild type at the time
150 when the DSB reached half of the peak height (11%; Figure 1D, dashed line). In
151 addition, the *pph3* mutants showed an accumulation of meiotic DSBs with hyper-
152 resected ends until 6 h after meiosis entry, resulting in an approximately 3 h delay in
153 DSB disappearance (Figure 1D). These observations indicated the necessity of PP4
154 phosphatase activity for timely DSB formation and turnover. It is reported that PP4-
155 dependent Rad53 dephosphorylation stimulates DNA end resection in mitotic DNA
156 damage response (VILLORIA *et al.* 2019). The opposite function of PP4 in the DSB end
157 resection may be due to mitotic and meiotic differences in Rad53 activity (CARTAGENA-
158 LIROLA *et al.* 2008).
159 Previous studies have revealed that PP4 is required for meiotic centromere
160 pairing. This was found to occur either through Zip1 dephosphorylation for Mec1-
161 mediated phosphorylation at S75 (KEOGH *et al.* 2006; FALK *et al.* 2010; HUSTEDT *et al.*
162 2015) or dephosphorylation of many other Mec1/Tel1 targets during DSB repair

163 (KEOGH *et al.* 2006; HUSTEDT *et al.* 2015). Thus, we constructed a mitotic cyclin *CLB2*
164 promoter-driven *MEC1* (p*CLB2-MEC1*) *tel1*Δ allele to determine the effect of Mec1 and
165 Tel1 on delayed DSB formation and/or turnover in the *pph3* mutants. It is known that
166 p*CLB2* induces mitosis-specific gene expression. Thus, it can be inferred that p*CLB2-*
167 *MEC1* causes meiosis-specific shutdown of *MEC1* transcription (LEE AND AMON 2003).
168 We confirmed that the effect of this construct is not different from that of the *mec1*Δ
169 *sml1*Δ strain in meiotic Hop1 phosphorylation. In addition, p*CLB2-MEC1* showed
170 significant lower spore viability (59.6 ± 4.6%) compared to the wild type (96.1 ± 1.8%,
171 $P < 0.0001$). This was found to be indistinguishable from *mec1*Δ *sml1*Δ (55.5 ± 7.1%, P
172 = 0.37) or other *MEC1*-defective alleles (Supplemental Figure 1A). The p*CLB2-MEC1*
173 *tel1*Δ cells showed a reduced level of meiotic DSB formation (7.7 ± 1.9% of total DNA)
174 compared to that in the wild type (22.7 ± 3.1%). p*CLB2-MEC1 tel1*Δ *pph3*Δ triple
175 mutant showed more severe reduction of DSB formation (5.3 ± 0.45%; Figure 1D,
176 graph). At later time points, in contrast to the *pph3* mutants, the p*CLB2-MEC1 tel1*Δ
177 and p*CLB2-MEC1 tel1*Δ *pph3*Δ mutants showed the timely disappearance of DSBs,
178 i.e., 6 h into meiosis (Figure 1D). These findings suggested that DSB accumulation and
179 the resulting delay in DSB repair, which was observed in the *pph3* mutants at later time
180 points (at 5–6 h), was dependent on Mec1/Tel1 (Figure 1E). By contrast, in the
181 initiation of DSB formation, the p*CLB2-MEC1 tel1*Δ *pph3*Δ triple mutant showed a peak
182 at 4 h, whereas the p*CLB2-MEC1 tel1*Δ double mutant peaked between 3 and 4 h after
183 onset of meiotic entry (Figure 1D, graph). As a delay in meiotic DSB formation in the
184 absence of Tel1/Mec1 activity was observed, the delayed DSB formation caused by
185 *pph3* mutations appeared to be independent of Mec1/Tel1.

186 Next, we analyzed hetero-duplex (HD) formation using Southern blot to
187 examine meiotic inter-homolog recombination products using heteroallelic restriction
188 enzyme sites *Mlu*I and *Bam*HI located near the DSB I site, and polymorphic *Xho*I sites
189 around the *HIS4-LEU2* hot spot (Figure 1C) (STORLAZZI *et al.* 1996). Corresponding to
190 the delayed meiotic DSB appearance and disappearance at the hot spot, the formation
191 of both HDs corresponding to intermediates for crossover (CO) and non-crossover
192 (NCO) were delayed by 3 h in the *pph3* mutants relative to that in the wild type (Figure
193 1E). In addition, an increase of NCO intermediates (HD1 and 4) at 8 h and a slight
194 reduction of CO intermediates (HD2 and 3) compared to that of the wild type were
195 observed not only in the *pph3*Δ, as reported previously (FALK *et al.* 2010), but also in
196 the *pph3-H112N* mutant (Figure 1E).
197 After DSB end resection, meiotic DSBs are recognized by recombinases
198 Rad51 and Dmc1, which facilitate strand exchange within the formation of COs and
199 NCOs. Cytological analysis revealed that Rad51appear transiently as punctate foci on
200 meiotic chromatin structure in the wild type (SHINOHARA *et al.* 2000). Thus, we next
201 examined the kinetics of Rad51 assembly and disassembly in the *pph3* mutants using
202 cytological analysis (Figure 1F). Results indicated that, there was a 1 h delay in the
203 Rad51 assembly among the *pph3* compared to that in the wild type. In addition,
204 accumulation of Rad51 foci was evident at 5 h after meiotic entry (Supplemental Figure
205 1C). In contrast, a significantly lower number of Rad51 foci per nucleus was observed
206 at an early time point (3 h) in the *pph3*Δ and *pph3-H112N* mutants compared to that in
207 the wild type (64 ± 2.7, 56 ± 2.7, and 49 ± 3.3, respectively; Figure 1F). This further
208 indicated that PP4, as well as its phosphatase activity, is required for the initiation of
209 meiotic DSB formation in proper timing. In the disassembly phase of Rad51 foci, a

210 significant reduction in the number of Rad51 foci per nucleus was observed in the wild
211 type. However, continuous accumulation of Rad51 foci was observed in the *pph3*
212 mutants corresponding to inefficient meiotic DSB repair.
213
214 **PP4 contributes to timely assembly of Hop1 onto chromatin independent from a**
215 **meiotic DSB dependent Mec1/Tel1 activity**
216 Hop1 is a meiosis-specific phosphorylation target of Mec1 and Tel1 (CARBALLO *et al.*
217 2008), and PP4 is involved in the dephosphorylation of Hop1 (CARBALLO *et al.* 2008;
218 FALK *et al.* 2010). Furthermore, Hop1 is a HORMA-domain protein and contributes to
219 the axis structure, in conjugation with Red1. Hop1 is essential for partner choice in
220 meiotic recombination (known as inter-homolog bias), and for efficient DSB formation
221 (HOLLINGSWORTH *et al.* 1990; NIU *et al.* 2005; PANIZZA *et al.* 2011; SUBRAMANIAN *et al.*
222 2016). Since it was observed that PP4 is required for efficient initiation of meiotic DSB
223 formation (Figure 1C and D), we analyzed the kinetics of Hop1 assembly onto
224 chromatin during meiotic prophase-I (Figure 2A). In the wild type, Hop1 assembly
225 began 2 h after the onset of meiosis, when is corresponding to leptotene and prior to
226 DSB formation.
227 We also analyzed the localization of Hop1, and Hop1 phosphorylation at
228 threonine 318 (Hop1-pT318) on meiotic chromatin. Hop1-pT318 is dependent on
229 Mec1/Tel1 kinase activation by Spo11-induced meiotic DSB formation (CARBALLO *et al.*
230 2008). Hop1-pT318 has been observed as punctate foci at the end of short patches of
231 Hop1 signal in the wild type (CARBALLO *et al.* 2008) (Figure 2A and B). In the wild type,
232 50% of the cells displayed Hop1 foci 2 h after meiosis entry, but few Hop1-pT318 were
233 observed at the same time. Hop1-pT318 foci began to appear after 3 h (Figure 2A and

234 B). Although the formation of Hop1-pT318 foci was dependent upon Spo11 function,
235 normal Hop1 assembly was also observed in the *spo11-Y135F*, which lacks the Spo11
236 catalytic tyrosine residue (Figure 2A and B). In addition, it is known that Hop1-pT318
237 focus formation requires single-stranded regions at meiotic DSB ends (IWASAKI *et al.*
238 2016). The approximately 2 h time lag evident between the Hop1 loading and the
239 Hop1-pT318 signals observed in the present study indicate that, in wild type, Hop1
240 assembly occurs prior to the DSB formation and/or DSB-end resection. In *pph3*
241 mutants, Hop1 assembly was rarely seen at 2 h compared to that in the wild type. After
242 2 h, Hop1 staining gradually increased, reaching the wild-type's frequency (80%) at 5
243 h. Notably, pT318 staining appeared at approximately the same time (3 h) as the
244 appearance of Hop1 foci (Figure 2A and B) and then gradually increased in ways
245 similar to Hop1, suggesting that Hop1 loading seemed to be the rate-limiting factor for
246 Hop1 phosphorylation in the *pph3* mutants. These results indicated that Pph3 and its
247 activity can promote the timely loading of Hop1 on chromosomes. We further confirmed
248 that this was not due to delayed expression of Hop1 in the mutants (see Figure 2C and
249 Supplemental Figure 2B). In addition, the delayed assembly of Hop1 in the *pph3*
250 mutants was observed in the *spo11-Y135F* mutation background (Figure 2A), thus
251 indicating that PP4 promotes Hop1 assembly independent of meiotic DSB formation.
252 Interestingly, Hop1 assembly in the *spo11-Y135F pph3-H112N* double mutant showed
253 a significant delay compared to that in the *pph3-H112N* mutant (Figure 2A). This would
254 suggest a parallel function of PP4 and Spo11 in Hop1 assembly or stabilization on the
255 chromosome axes.
256 Spo11 independent PP4 function in Hop1 assembly suggests a possibility that
257 meiotic DSB-dependent Mec1/Tel1 activation is not essential to PP4 function in Hop1

258 assembly. In contrast, the *pph3* mutant shows a Mec1-dependent meiotic DNA
259 replication delay (FALK *et al.* 2010). Further, we confirmed delayed meiosis progression
260 in the *spo11-Y135F pph3-H112N* double mutant as reported by Falk et al
261 (Supplemental Figure 2A). We subsequently examined the effect of Mec1 and Tel1 on
262 Hop1 assembly in *pph3*Δ mutants. Although p*CLB2-MEC1 tel1*Δ mutant cells did not
263 display any defects in Hop1 assembly, the p*CLB2-MEC1 tel1*Δ *pph3*Δ mutant showed
264 delayed Hop1 assembly, similar to the *pph3* mutants (Figure 2A and B). In contrast,
265 although a few faint Hop1-pT318 foci were observed in the p*CLB2-MEC1 tel1*Δ
266 mutation background, none were found in the *spo11-Y135F* mutation background
267 (Figure 2B). This Hop1-pT318 focus formation raises doubts as to the presence of
268 residual Mec1 activity in the p*CLB2-MEC1* meiosis-specific shout down allele.
269 However, Hop1-pT318 foci in strains with p*CLB2-MEC1 tel1*Δ mutation backgrounds
270 were qualitatively distinguishable from those in the strains with wild-type *MEC1*
271 background (Figure 2C).
272 Next, we analyzed the phosphorylation status of target proteins of PP4 during
273 meiosis using western blot. PP4 is known to be involved in dephosphorylation of S129
274 of histone H2A (γH2A) after DNA damage in vegetative growth cells (KEOGH *et al.*
275 2006), as well as in Hop1-pT318 during meiosis (CHUANG *et al.* 2012). Thus, we first
276 confirmed that the γH2A signal accumulated in the *pph3* mutants during meiosis in a
277 Mec1/Tel1 dependent manner, a pattern similar to that in mitotic cells, with markedly
278 reduced γH2A signals in the p*CLB2-MEC1 tel1*Δ *pph3*Δ mutant (Figure 2D). Moreover,
279 accumulation of Hop1-pT318 signal was observed until the 8 h point in the *pph3*Δ
280 mutant. The presence of this phosphorylation depended upon Mec1/Tel1 (Figure 2D).
281 Although Hop1 protein production was detectable from 2 h after meiosis entry in both

282 wild-type and *pph3* mutants, it was slight delayed in the *pph3* mutants. By contrast, the
283 initiation of Hop1 phosphorylation at T318 was delayed by 1 h in the *pph3* mutants
284 before reaching maximum levels compared to that in the wild type. Notably, despite the
285 timely early production of Hop1 protein in the *pph3* mutants (Figure 2D and
286 Supplemental Figure 2B), the appearance of Hop1 foci on meiotic nuclear spread was
287 significantly delayed in the *pph3* mutants (Figure 2A). This suggested that, although
288 PP4 might not be largely involved in Hop1 production, it acted to promotes Hop1
289 loading onto chromatin. Moreover, Hop1 protein production kinetics were also normal
290 in the p*CLB2-MEC1 tel1*Δ or p*CLB2-MEC1 tel1*Δ *pph3*Δ mutants. In contrast to finding
291 for γH2A phosphorylation, residual Hop1-pT318 signal was not detected in the p*CLB2-*
292 *MEC1 tel1*Δ background. This observation accorded with a previous report showing
293 that Hop1 phosphorylation largely depends on Mec1 and Tel1 activities (CARBALLO *et*
294 *al.* 2008). Overall, our findings indicate a defect in Hop1 assembly on chromatin,
295 despite sufficient production of Hop1 protein.
296
297 **PP4 is involved in Red1-Hop1 complex assembly but not in meiotic cohesin**
298 **assembly**
299 Next, we examined Red1 and Rec8 meiotic chromosome axis components (ROCKMILL
300 AND ROEDER 1988; KLEIN *et al.* 1999). Red1 forms a complex with Hop1 (NIU *et al.*
301 2005). Rec8 is a component of the meiosis-specific sister chromatid cohesin complex.
302 Both proteins are required for the proper formation of both the meiotic axial elements,
303 as well as a highly-ordered specific chromosome structure, termed the SC (KLEIN *et al.*
304 1999). Red1 and Rec8 are mutually independently recruited to chromatin (SUN *et al.*
305 2015). We examined Red1 and Rec8 staining on meiotic chromatin (Figure 3A). Wild

306 type, Red1 and Rec8 colocalized with each other and formed linear structures along
307 the 4′,6-diamidino-2-phenylindole (DAPI) nuclear signal on meiotic chromatin 3 h after
308 meiosis entry. This co-stain pattern on Rec8 and Red1 differs slightly from previous
309 reports (KIM *et al.* 2010). This may be due to differences in the antibodies used. By
310 contrast, in the *pph3* mutants, Red1 and Rec8 were observed as many fine signals
311 throughout the chromatin spreads. The number of Rec8 signals was clearly higher than
312 that of Red1. Time course experiments revealed a significant delay in the assembly of
313 Red1 protein in the *pph3* mutants, similar to the assembly of Hop1 shown in Figure 2A
314 and 2B. However, the timing of Rec8 assembly, despite of its unique structure, was not
315 affected in the presence or absence of Pph3 activity (Figure 3B). An additional delay in
316 the disassembly of both Red1 and Rec8 was observed in the *pph3* mutants.
317 Next, we analyzed Red1 and Rec8 protein production during meiosis using
318 western blot (Figure 3C). Rec8 phosphorylation via Dbf4-dependent kinase (DDK) and
319 polo-like kinase 1 (PLK1) is associated with cleavage-independent cohesion release
320 from late prophase-I chromatin (CHALLA *et al.* 2019). Although Rec8 appeared at
321 approximately the same time in the *pph3* mutants as in the wild type, the
322 phosphorylation of Rec8 was delayed in the *pph3* mutants compared to in the wild
323 type. Corresponding to delayed Rec8 phosphorylation, Rec8 cleavage that occurs
324 during the meiotic divisions was also delayed in the *pph3* mutants. These results were
325 consistent with delayed meiosis progression in *pph3* mutants (Supplemental Figure
326 2A). In addition, normal levels of Red1 protein were observed in *pph3* mutants (Figure
327 3C). These results suggest that PP4 is essential to properly timed Hop1-Red1 loading,
328 but not Rec8 cohesin, which is solely required for basic axis structure construction.
329

330 **PP4 physically interacts with Hop1 protein**

331 We next examined physical interactions between the Hop1-Red1 and PP4 using a co-
332 immunoprecipitation assay (Figure 4A). Psy2-13Myc protein was precipitated using
333 anti-Myc antibody in meiotic cell extracts of *PSY2-13MYC* derivative *PPH3* (wild type)
334 cells. The Hop1 signal was detected in the whole cell extracts (WCEs) at 2 to 6 h
335 during meiosis. After immunoprecipitation in *PSY2-13MYC* cell extracts, the Hop1
336 protein signal was observed at 2 and 4 h after meiosis entry, indicating the interaction
337 of Pys2 with Hop1. However, despite of the presence of Hop1 protein in the WCEs, the
338 signal was not apparent at 6 h. Since Hop1-PP4 physical interaction was detected, we
339 analyzed other axis component Red1 and Rec8 proteins in the precipitates using
340 western blot. By contrast, Red1 and Rec8 were not observed in the precipitates, even
341 though both proteins were present in the WCEs. The findings indicate that PP4
342 primarily interacts with Hop1, but not Red1 or Rec8. Given that Hop1 binds to Red1 as
343 a complex (NIU *et al.* 2005), there might be two distinct populations of Hop1, Hop1-PP4
344 and Hop1-Red1.

345

346 **Defective Hop1 assembly onto chromosome axes in the *pch2*Δ background in**
347 **the *pph3* mutant**

348 Pch2 is a AAA+ ATPase that promotes Hop1 turnover from synapsed chromosome
349 axes. It is known to be abundant localization of Hop1 protein on the synapsed axes in
350 *pch2*Δ cells. Pch2 is also involved in a Hop1 dephosphorylation (LO *et al.* 2014;
351 HERRUZO *et al.* 2016; SUBRAMANIAN *et al.* 2016). Given our observation a defect in
352 Hop1 assembly and delayed phosphorylation of Hop1 in the *pph3* mutants, we

353 analyzed the effects of the *pph3* mutations in the Hop1 assembly onto meiotic
354 chromosome axis in the *pch2*Δ background.
355 First, spore viability and distribution of viable spores were analyzed in the
356 *pph3*Δ *pch2*Δ double mutant using tetrad analysis (Figure 4B). Spore viability in the
357 wild type, *pph3*Δ, and *pch2*Δ was 97%, 88%, and 91%, respectively. Both *pph3*Δ and
358 *pch2*Δ had slightly reduced spore viability, but there was no significant bias in the
359 distribution of viable spores in asci, as reported previously (SAN-SEGUNDO AND ROEDER
360 1999; FALK *et al.* 2010). By contrast, the spore viability of the *pph3*Δ *pch2*Δ double
361 mutant was only 25%, with distributions of 0-, 2-, and 4-viable spores. This bias was
362 indicative of the non-disjunction of homologous chromosomes in the first meiotic
363 division.
364 In Hop1 and Hop1-pT318 assembly/disassembly kinetics, Hop1-pT318
365 assembly was delayed in the *pch2*Δ mutant, consistent with a delayed meiotic DSB
366 formation (FARMER *et al.* 2012). This delay was similar to that in the *pph3*Δ and the
367 *pph3*Δ *pch2*Δ double mutants (Figure 4C and D). Thus, indicating the absence of
368 additive defects to *pph3*Δ in Hop1 assembly/disassembly in the *pch2*Δ mutation. The
369 findings suggest that Pch2 and PP4 function in the same pathway in Hop1
370 assembly/disassembly.
371 Next, we examined the effect of the *pch2*Δ mutation on Hop1 localization by
372 using cytological analysis. As indicated previously (IWASAKI *et al.* 2016) and in Figure
373 2A, Hop1-pT318 foci were observed as punctate foci in the wild type and were affected
374 in the *pph3*Δ in early prophase-I (approximately 3 h in meiosis) (Figure 4D). In the
375 *pch2*Δ mutant, Hop1 aggregates colocalized with Hop1-pT318 signals. Similar
376 aggregates were noted in the *pph3*Δ *pch2*Δ double mutant at an early time point.

377 Notably, at the later time point (6 h during meiosis), Hop1-pT318 signals were
378 observed as a beaded chain on the fully elongated Hop1 signal on meiotic
379 chromosomes in the *pch2*Δ mutant cells (Figure 4D). In the *pph3*Δ *pch2*Δ double
380 mutant, some Hop1 signals were observed as dots and some were colocalized with the
381 Hop1-pT318 signal, similarly to that in *pph3*Δ. These findings suggest that the *pph3*Δ
382 mutation is epistatic to the *pch2*Δ mutation in Hop1 localization process. This further
383 indicates that PP4 may function to promote Hop1 assembly onto meiotic chromatin that
384 lends to construction of the chromosome axis, a process occurring prior to Pch2
385 function in Hop1 removal from the chromosome axis. By contrast, in the *pph3*Δ *pch2*Δ
386 double mutant, some Hop1-pT318 signals were observed as beaded chain on fully
387 elongated Hop1. This indicates that the *pch2*Δ mutation stabilized Hop1 protein in the
388 *pph3*Δ on some chromosome axis, but not on others. Thus, other pathways may be
389 able to promote Hop1 assembly in the absence of PP4.
390
391 **Multiple pathways to promote Hop1 assembly**
392 On the meiotic chromosome axes, Hop1 is dynamic and is removed from
393 chromosomes through Pch2 activity. Then, Hop1 is ultimately replaced by the
394 transverse element component Zip1 in the pachytene (BORNER *et al.* 2008). Given this,
395 we examined Zip1 localization in the *pph3*Δ *pch2*Δ double mutant. In wild-type cells, as
396 previously reported, Zip1 was observed as dotty foci in the leptotene (2 h). It begins to
397 elongate after the DSB end resection in the zygotene, followed by the extension of Zip1
398 throughout each chromosome in the pachytene (SYM *et al.* 1993; STORLAZZI *et al.*
399 1996; SHINOHARA *et al.* 2015). Significant delays in both the appearance of dotty Zip1
400 signals and the Zip1 elongation were evident for *pph3*Δ (Figure 5A), as reported

401 previously (FALK *et al.* 2010). The *pch2*Δ mutant showed Zip1 elongation delay, in
402 addition to issociation from the chromosomes after full elongation. However, the
403 elongated Zip1 became the major population at 5 h after meiosis entry. In the *pph3*Δ
404 *pch2*Δ double mutant, after the delayed appearance of dotty Zip1 signals, similar to
405 *pph3*Δ (2 to 3 h), compromised Zip1 elongation was observed. Complementary
406 localization of Zip1 and Hop1 on chromosomes was observed from zygotene to
407 pachytene in wild type. A similar localization pattern was evident in the *pph3*Δ mutant.
408 By contrast, *pch2*Δ mutant cells showed uniform colocalization of Zip1 and Hop1
409 (Figure 5B), as previously reported (BORNER *et al.* 2008). *Saccharomyces cerevisiae*
410 haploid cells have 16 chromosomes. Theoretically, 16 bivalents should be observed in
411 the pachytene stage. However, the number of linear Zip1 signals per cell was 12 ± 2.7
412 (mean ± 95% confidence interval) in the *pch2*Δ. This amout was significantly reduced
413 in the *pph3*Δ *pch2*Δ double mutant in 68% of *pch2*Δ (8.2 ± 2.6) (Figure 5B and C).
414 Although several elongated Zip1 signals colocalized with Hop1 in *pph3*Δ *pch2*Δ, Hop1-
415 Zip1 free DAPI signals were also often observed in *pph3*Δ *pch2*Δ (Figure 5B). Next, we
416 compared the length of a linear stretch of Zip1-Hop1 signals indicative of chromosome
417 size in *pch2*Δ within *pph3*Δ *pch2*Δ, as specifically observed in the process of residual
418 Zip1-Hop1 elongation in *pph3*Δ *pch2*Δ. No significant difference was evident (P = 0.19,
419 Figure 5D).

420 The *pph3*Δ mutation showed a chromosome-dependent effect in Hop1-Zip1
421 elongation in the *pch2*Δ mutant background. We therefore analyzed Rec8 and Red1
422 localization, as alternative axis components, to determine the status of the Hop1-Zip1
423 free region observed in the *pph3*Δ *pch2*Δ double mutant. Unlike the Hop1 protein on
424 the axes, Red1 is not therefrom by Pch2. In addition, Rec8 is recruited to chromatin

425 independent of Hop1-Red1 (SUN *et al.* 2015). Further, Rec8 focus formation was not
426 affected in the *pph3* mutants (Figure 3A). In *pch2*Δ mutant cell, Rec8 and Red1
427 evidently colocalized on the chromosome axes (Figure 5E). In contrast, in the *pph3*Δ
428 *pch2*Δ double mutant, Rec8 and Red1 only colocalized on the synapsed chromosome
429 axes. Further, many of the Rec8 was observed as a thin bead chain, where are not
430 synapsed. These findings suggest that the *pph3* mutants are defective primarily at the
431 Red1-Hop1 recruitment stage in the formation of the pre-Zip1 recruited chromosomal
432 axis.
433
434 **Delayed meiosis progression in the *pph3*Δ occurs independent of Pch2**
435 Hop1 is an adaptor of the meiosis-specific prophase checkpoint. Hop1
436 phosphorylation is affected in the *pch2*Δ mutant (LO *et al.* 2014) and Mec1/Tel1-
437 dependent phosphorylation of Hop1 affects Hop1 activity (CARBALLO *et al.* 2008). In the
438 wild type, Hop1 phosphorylation was detected during meiosis starting at 3 h and
439 continued until 5 h, upon which point, it disappeared (Figure 5F). The timing of this
440 Hop1-pT318 disappearance aligned with the timing of meiosis-I initiation (Figure 5G).
441 This was also observed with *pph3*Δ mutant cells, in which the Hop1-pT318 signal
442 disappeared at 8 h simultaneously with the appearance of post-meiotic cells. In *pch2*Δ
443 mutant cells, consistent with previous findings, Hop1 protein accumulated until 10 h,
444 and stimulated Hop1 phosphorylation disappeared by 8 h. In contrast, in the *pph3*Δ
445 *pch2*Δ double mutant, Hop1 protein accumulated until 10 h. In turn, Hop1-pT318 signal
446 also accumulated until 8 h after which it began to disappear. Notably, corresponding to
447 the delayed disappearance of the Hop1-pT318 signal, the *pph3*Δ *pch2*Δ double mutant
448 showed severe delay in meiosis progression (Figure 5F and G). The *pch2*Δ mutation

449 suppresses pachytene arrest in the *zip1* mutant (SAN-SEGUNDO AND ROEDER 1999;

450 BORNER *et al.* 2008). It, however, cannot suppress the delayed progression of meiosis

451 in the *pph3*Δ mutant. Thus, this delay in *pph3*Δ can be caused by a mechanism

452 different mechanism from that observed in the *zmm* mutant.

453

454

455 **Discussion**

456

457 During meiotic recombination, the chromosome axis serves as an essential scaffold.
458 Some components, including Mer2 and Rec8, are associated with pre-meiotic DNA
459 replication. In contrast, the molecular mechanism underlying the formation of highly
460 organized chromosomal axis structure, especially, the initial step of Hop1 recruitment
461 onto meiotic chromatin, is not well understood. The results of this study support
462 indications that PP4 may function in Hop1 recruitment onto chromatin in the initiation
463 step of chromosome axis formation in early meiotic prophase-I.

464

465 **PP4 is involved in Hop1 recruitment onto chromatin independently from meiotic**
466 **DSB-induced Tel1/Mec1 kinase activity**

467 Significant delays in Hop1-Red1 loading were observed in *pph3* mutants, *pph3*Δ and
468 *pph3-H112N*. In contrast, the timings of the production of Hop1 protein and the
469 assembly meiotic cohesin component Rec8 in *pph3* mutants were indistinguishable
470 from those in wild type. Delayed loading of Hop1 was also observed in the absence of
471 Mec1 Tel1 activity and meiotic DSB formation. These results suggest PP4 is involved
472 in Hop1 assembly before meiotic DSB formation. It has been reported that PP4
473 mutants show a delay in completing pre-meiotic DNA replication (FALK *et al.* 2010).
474 Thus, our results cannot completely exclude the possibility that delayed completion of
475 pre-meiotic DNA replication leads to subsequent delayed axis formation. It has been
476 reported Rec8 loading is linked to pre-meiotic DNA replication (KUGOU *et al.* 2009).
477 There was a slight delay in Rec8 loading in the *pph3*Δ (but not in the *pph3-H112N*
478 mutant), and this delay was less affected compared to Red1 loading (Figure 3B). From

479 these results, we concluded that PP4 functions in promoting Hop1 loading during
480 chromosome axis formation, an observation reached in light of the indirect pre-meiotic
481 DNA replicative effects of its function as well.
482 During the formation of the meiotic SC structure, PP4 is also required for
483 centromere-mediated chromosome pairing through Zip1 phosphorylation in a
484 Mec1/Tel1-dependent manner (FALK *et al.* 2010). Both *pph3* mutants displayed
485 significant delays in Hop1 assembly onto chromatin. However, this delay was
486 Tel1/Mec1-independent (Figure 2A and B). Therefore, the observed Hop1 assembly
487 delay would not be caused by compromised centromere pairing. In *pph3* mutants, the
488 appearance of γH2A which is phosphorylated by Mec1/Tel1 kinase was observed at
489 the same timing as that in wild type. By contrast, Tel1/Mec1-induced Hop1
490 phosphorylation (Hop1-pT318) was delayed. This result supports the idea that delayed
491 Hop1 phosphorylation is caused by the delayed assembly of Hop1 onto the axes.
492 Notably, *pph3* mutation-dependent delay in Hop1 phosphorylation was observed, not
493 only in p*CLB2-MEC1*, but also in the *mec1*Δ backgrounds (Supplemental Figure 1A).
494 This suggests that PP4 promotes timely recruitment of Hop1 onto chromatin
495 independent of Mec1 (or Mec1 / Tel1) activity, rather than the indirect effects of Mec1-
496 PP4-related premeiotic S-phase defects. Since Hop1 chromatin loading is one of the
497 rate-determining factors that promotes meiotic DSB formation (PANIZZA *et al.* 2011),
498 delayed DSB formation and Rad51 loading in the *pph3* mutant would also be caused
499 by this delayed Hop1 loading onto the axes. In addition, our study has revealed the
500 physical interaction between the Hop1 and a PP4 component, indicating that the Hop1
501 protein in the precipitates was not always phosphorylated (Figure 4A). These findings

502 suggest that the Hop1-PP4 interaction may not only occur for enzymatic activity but
503 may also regulate Hop1 assembly.
504 Another possibility is that delayed observation of Hop1 localization on the
505 chromosome axes, in the absence of PP4, is unstable and thus rapidly removed from
506 the axes. To assess this, we examined Hop1 localization in the absence of Pch2.
507 Proper Hop1 assembly did not occur in 32% of the chromosomes in each nucleus of
508 *pph3*Δ *pch2*Δ double mutant (Figure 5C). This strongly suggests that PP4 is involved in
509 the recruitment phase of Hop1 and not in its stabilization on the chromosome axes.
510 Conversely, 68% of chromosomes in the same nucleus displayed stable Hop1
511 assembly by *pch2*Δ, even in *pph3*Δ. These observations indicate that multiple
512 pathways, beyond the PP4 alone, can promote Hop1 assembly.
513
514 **What molecular mechanism promotes PP4 induced Hop1 assembly?**
515 The molecular mechanism by which PP4 promotes Hop1 assembly is still unknown.
516 Furthermore, at this point, it is not clear whether the effect of PP4 on axis formation is a
517 direct or indirect effect.
518 Hop1 is a HORMA-domain protein. The dynamics of C-terminal "closure-motif"
519 may be important for chromosome axis assembly and disassembly through Red1
520 interaction. In addition, substitution of K593 of Hop1 with alanine (*hop1-K593A*) results
521 in severe defects in the Red1 interaction (WEST *et al.* 2018). We identified *hop1-S595L*
522 mutant which showed hypomorphic Hop1 function defects such as normal spore
523 viability and Hop1 assembly, but reduced Hop1 protein production, slightly delayed
524 Hop1 phosphorylation at T318 and meiosis-I progression (Supplemental Figure 4A).
525 We analyzed Hop1 assembly onto chromatin in the *pph3* within the *hop1-S595L*

526 mutation background. The *pph3* and the *hop1-S595L* mutations showed a synergistic
527 defect, thus *HOP1* and *PPH3* showed a genetic interaction in Hop1 assembly
528 (Supplemental Figure 4B).
529 In addition, a delay in Hop1 assembly in the *pph3* mutant was also observed in
530 the p*CLB2-MEC1 tel1*Δ and *spo11-Y135F* background, and Pph3 catalytic activity was
531 required for timely recruitment of Hop1 onto chromatin (Figure 2A and B). These
532 observations indicate PP4 dephosphorylation of unknown target protein before meiotic
533 DSB formation is required for appropriately timed, Hop1 assembly onto chromatin
534 (Figure 6). Since Hop1-PP4 physical interaction was detected simultaneously with
535 Hop1 recruitment in the wild type (at 2 h; Figure 4A), Hop1 may be one of the most
536 probable target for dephosphorylation by PP4 in the recruitment process. In contrast,
537 the candidate protein kinase(s) regulating Hop1 assembly are DDK and/or CDK.
538 However, the ATP analog sensitive *cdc7* allele (*cdc7-as3*) reportedly showed normal
539 Hop1 production, despite a lack of Hop1 phosphorylation, in the presence of an ATP
540 analog (WAN *et al.* 2006). The focus formation of Cdc28 (a component of CDK) on
541 meiotic chromatin are dependent upon Hop1, Red1 and Rec8, but not on Mek1/Mre4.
542 The analog sensitive allele *cdc28-as1* reportedly displayed compromised Rad51 focus
543 formation and severe defects in Zip1 elongation. However it did not affect Red1 loading
544 in the presence of an ATP analog (ZHU *et al.* 2010). These findings indicate that CDK
545 and DDK functions are associated with Hop1 function. However, direct phosphorylation
546 of Hop1 by CDK and/or DDK has not been reported. There are two predicted CDK
547 phosphorylation motifs (S/T-P) in Hop1: S494 and S531 (ZHU *et al.* 2010). The
548 presence of sequential phosphorylation by CDK followed by DDK in the sequence of
549 serine/threonine residues in addition to the CDK phosphorylation motif has been

550 described for related target proteins such as Mer2 (WAN *et al.* 2006) and Mps3 (RAO *et*
551 *al.* 2020). Furthermore, the S494 of Hop1 overlaps this motif (T-S-^{494}S-P). In addition,
552 the possibility remains that Tel1/Mec1 kinase activity during the premeiotic S-phase is
553 involved in the promotion of Hop1 loading.
554
555 **PP4 has an independent role from ZMM/SIC components in the prophase**
556 **checkpoint**
557 Pch2 activates the meiotic prophase checkpoint when meiotic DSB repair or
558 chromosome synapsis is compromised in *zip1*, *zip2*, or *dmc1* mutant cells (SAN-
559 SEGUNDO AND ROEDER 1999; BORNER *et al.* 2008). Prior studies have reported that the
560 PP4 mutant shows a *zmm* mutant-like phenotype in several processes, including
561 meiotic recombination, NCO/CO ratio aberration, temperature-sensitive meiosis
562 progression, CO formation, and compromised CO interference (BORNER *et al.* 2004;
563 FALK *et al.* 2010). In addition, defective CO formation in *pph3*Δ is epistatic to *msh4*Δ
564 (FALK *et al.* 2010). We also observed compromised CO and elevated NCO formation
565 via HD analysis (Figure 1C). These are commonly observed in *zmm* mutants
566 (SHINOHARA *et al.* 2008). Moreover, although *pch2*Δ suppresses meiotic prophase
567 arrest of *zmm* mutants (SAN-SEGUNDO AND ROEDER 1999), it could not suppress the
568 delayed meiosis progression of the *pph3*Δ mutant. These findings suggest that delayed
569 meiosis progression is caused by a different mechanism from that of *zmm* or *dmc1*
570 mutants. It was rrecently eported that Pch2, in collaboration with Hop1, mediates the
571 meiotic prophase checkpoint (RAINA AND VADER 2020; HERRUZO *et al.* 2021). In *pph3*
572 mutants, compromised synapsis as well as inefficient meiotic recombination easily
573 activate the meiotic prophase checkpoint because of enhanced Mec1/Tel1 signaling.

574 However, the checkpoint signal was not restored even in the absence of Pch2. In
575 addition, we also observed delayed meiosis progression in *pph3* mutants without
576 meiotic DSB formation in the *spo11-Y135F* background (Supplemental Figure 2A). This
577 could be caused by insufficient Hop1 loading on the chromosome axis or an
578 accumulation of unbound inactive form of Hop1 protein. Further, PP4 might be involved
579 in inactive to active conversion of Hop1 before chromatin loading, thus ensuring proper
580 axis construction (Figure 6).
581

582 **Materials and Methods**

583 **Yeast strains and media**

584 All the yeast strains and their genotypes are listed in Supplemental table 1. We used
585 isogenic *S. cerevisiae* SK1 background NKY1551 derivatives (STORLAZZI *et al.* 1996).
586 *PPH3-13MYC* was constructed using a polymerase chain reaction–based tagging
587 method (BAHLER *et al.* 1998). *pph3-H112N* was constructed vis two-step gene
588 replacement. YPAD (1% yeast extract, 2% Bacto peptone, 0.01% adenine, 2%
589 glucose), SPM (0.3% potassium acetate, 0.03% raffinose), and DISS plates (YPAD
590 medium containing 2.4% Bacto Agar) were used.

591

592 **Yeast meiosis time course**

593 The experiments were performed as described previously (SHINOHARA *et al.* 2003).
594 Meiosis progression was analyzed by counting the number of nuclei in each ascus at
595 each time point. Nuclei were visualized by staining with 4', 6-diamidino-2-phenylindole,
596 dihydrochloride (DAPI) and observed under an epifluorescence microscope
597 (AxioSkop2, Carl Zeiss). More than 100 nuclei were analyzed at each time point.

598

599 **Cytological analysis**

600 Immunostaining of yeast meiotic nuclear spreads was performed as previously
601 described (SHINOHARA *et al.* 2015). Stained samples were observed under
602 epifluorescence using the Axioskop 2 microscope equipped with light-emitting diode
603 fluorescence light sources (X-Cite; Excelitas Technologies) and a 100× objective
604 (AxioPlan, NA1.4, Carl Zeiss). Images were captured with a CCD camera (Retiga;
605 Qimaging) and processed using iVision (BioVision Technologies) and Photoshop

606 (Adobe). The antibodies used in these assays were anti-Hop1 (IWASAKI *et al.* 2016)
607 (guinea pig, 1:500) , anti-Hop1-pT318(IWASAKI *et al.* 2016) (rabbit, 1:500), anti-Red1
608 (chicken, 1:500) (SHINOHARA *et al.* 2008) and anti-Rec8 (rabbit, 1:1000) (ZHU *et al.*
609 2010). Nuclei containing more than five foci were counted as focus-positive.
610
611 **Southern blot to detect meiotic DSBs and recombination intermediates**
612 Genomic DNAs prepared from yeast meiosis time course experiments were digested
613 with *Mlu*I, *Bam*HI, and *Xho*I for heteroduplexes (HDs), and *Pst*I for meiotic DSBs.
614 Probes for Southern blotting included: Probe 155 for HD and Probe 291 for DSB
615 detection (STORLAZZI *et al.* 1996; SHINOHARA AND SHINOHARA 2013). They were labeled
616 with α-^{32}P- dATP (NEG512H, PerkinElmer) using the random primer method (Random
617 Primer 6, NEB S1230S, Klenow fragment (3'-5' exo-, M0210) and visualized by using
618 FLA7000 (Cytiva). The visualized signals were analyzed using Image Quant TL
619 software (Cytiva) and images were processed using Photoshop (Adobe).
620
621 **Western blotting**
622 Western blotting was performed as described previously (SHINOHARA *et al.* 2015).
623 Meiotic yeast cell extracts were prepared by cell disruption using a Multi-Beads Shocker
624 (YASUIKIKAI) after trichloroacetic acid treatment. The primary antibody signal was
625 visualized using Alexa Fluor 680–labeled secondary antibodies (Thermo Fisher
626 Scientific) or IRDye 800CW–labeled secondary antibodies (LI-COR Biosciences) using
627 an Odyssey infrared imaging system (LI-COR Biosciences). Images were processed
628 using Photoshop (Adobe). The primary antibodies used in these assays were anti-
629 γH2A (anti-γH2A, AF2288, R&D Systems, 1:1000), anti-Myc (MC045, Nacalai Tesque,

630 1/1000), anti-Hop1 (guinea pig, 1/5000)(IWASAKI *et al.* 2016), anti-Hop1-pT318 (rabbit,
631 1/5000) (IWASAKI *et al.* 2016), anti-Rec8 (rabbit, 1/10000) (ZHU *et al.* 2010), anti-Red1
632 (chicken, 1/3000) (SHINOHARA *et al.* 2008) and anti-α-tubulin (YL1/2, Santa Cruz
633 Biotechnology, 1/3000). Tubulin signals were visualized using the LI-COR Bioscience
634 system or alkaline phosphatase stain (BCIP-NBT solution kit, Nacalai Tesque) on the
635 same membrane on which other meiotic proteins were detected.
636
637 **Immunoprecipitation**
638 The immunoprecipitation assay was performed as previously described with minor
639 modifications (SHINOHARA *et al.* 2008). Psy2-13Myc was immunoprecipitated using
640 anti-Myc antibody (MC045, Nacalai Tesque) These were bound to Dynabeads Protein
641 G (Thermo Fisher Scientific) from meiotic yeast cell lysate prepared using a Multi-
642 Beads Shocker (YASUIKIKAI) in lysis buffer (50 mM HEPES-NaOH, pH7.5, 150 mM
643 NaCl, 20% glycerol, 1 mM Sodium orthovanadate, 60 mM β-glycerophosphate, 0.1%
644 Nonidet P-40, 1:100 dilution of protease inhibitor cocktail (SIGMA-Aldrich) at the
645 indicated time points in Figure 4A and 4B. Psy2-13Myc, Hop1, Red1 and Rec8 proteins
646 in the precipitates and WCEs were detected as described in the western blot section.
647
648 **Tetrad analysis**
649 Tetrad analysis was performed as described previously (CHALLA *et al.* 2019). Parental
650 haploid strains were mated for 12 h on YPAD plates at 30°C and then transferred onto
651 SPM plates. After incubation at 30°C for 48 h, tetrads were dissected onto DISS plates
652 and incubated for 48 h.
653

654 **Data availability**

655

656 Strains and plasmids are available upon request.

657 The authors affirm that all data necessary for confirming the conclusions of the article

658 are present within the article, figures, and tables.

659

Acknowledgements

We are grateful to Dr. K. Matsuzaki, Dr. F. Klein, Dr. S. Gasser, and the members of the Shinohara lab for their helpful discussions. We thank Ms. A. Murakami and Ms. A. Kitada for their excellent technical assistance. K.L. was supported by a Fellowship from the Institute for Protein Research, Osaka University. We would like to especially thank Dr. A. Shinohara and Dr. K. Matsuzaki for critical reading of the manuscript. This work was supported by JSPS KAKENHI (#15H05973, #19K22402) and Takeda Science Foundation and was performed in part under the Cooperative Research Program of the Institute for Protein Research, Osaka University, CR-17-05.

670 **References**

671

672 Anderson, C. M., A. Oke, P. Yam, T. Zhuge and J. C. Fung, 2015 Reduced Crossover
673 Interference and Increased ZMM-Independent Recombination in the Absence of
674 Tel1/ATM. PLoS Genet 11: e1005478.
675 Bahler, J., J. Q. Wu, M. S. Longtine, N. G. Shah, A. McKenzie, 3rd *et al.*, 1998
676 Heterologous modules for efficient and versatile PCR-based gene targeting in
677 Schizosaccharomyces pombe. Yeast 14: 943-951.
678 Bishop, D. K., 1994 RecA homologs Dmc1 and Rad51 interact to form multiple nuclear
679 complexes prior to meiotic chromosome synapsis. Cell 79: 1081-1092.
680 Bishop, D. K., D. Park, L. Xu and N. Kleckner, 1992 DMC1: a meiosis-specific yeast
681 homolog of E. coli recA required for recombination, synaptonemal complex
682 formation, and cell cycle progression. Cell 69: 439-456.
683 Blat, Y., R. U. Protacio, N. Hunter and N. Kleckner, 2002 Physical and functional
684 interactions among basic chromosome organizational features govern early steps
685 of meiotic chiasma formation. Cell 111: 791-802.
686 Borner, G. V., A. Barot and N. Kleckner, 2008 Yeast Pch2 promotes domainal axis
687 organization, timely recombination progression, and arrest of defective
688 recombinosomes during meiosis. Proc Natl Acad Sci U S A 105: 3327-3332.
689 Borner, G. V., N. Kleckner and N. Hunter, 2004 Crossover/noncrossover
690 differentiation, synaptonemal complex formation, and regulatory surveillance at
691 the leptotene/zygotene transition of meiosis. Cell 117: 29-45.
692 Carballo, J. A., A. L. Johnson, S. G. Sedgwick and R. S. Cha, 2008 Phosphorylation of
693 the axial element protein Hop1 by Mec1/Tel1 ensures meiotic interhomolog
694 recombination. Cell 132: 758-770.
695 Carballo, J. A., S. Panizza, M. E. Serrentino, A. L. Johnson, M. Geymonat *et al.*, 2013
696 Budding yeast ATM/ATR control meiotic double-strand break (DSB) levels by
697 down-regulating Rec114, an essential component of the DSB-machinery. PLoS
698 Genet 9: e1003545.
699 Cartagena-Lirola, H., I. Guerini, N. Manfrini, G. Lucchini and M. P. Longhese, 2008
700 Role of the Saccharomyces cerevisiae Rad53 checkpoint kinase in signaling
701 double-strand breaks during the meiotic cell cycle. Mol Cell Biol 28: 4480-
702 4493.

Challa, K., V. G. Fajish, M. Shinohara, F. Klein, S. M. Gasser *et al.*, 2019 Meiosis-specific prophase-like pathway controls cleavage-independent release of cohesin by Wapl phosphorylation. PLoS Genet 15**:** e1007851.

Chuang, C. N., Y. H. Cheng and T. F. Wang, 2012 Mek1 stabilizes Hop1-Thr318 phosphorylation to promote interhomolog recombination and checkpoint responses during yeast meiosis. Nucleic Acids Res 40**:** 11416-11427.

De Muyt, A., A. Pyatnitskaya, J. Andreani, L. Ranjha, C. Ramus *et al.*, 2018 A meiotic XPF-ERCC1-like complex recognizes joint molecule recombination intermediates to promote crossover formation. Genes Dev 32**:** 283-296.

Falk, J. E., A. C. Chan, E. Hoffmann and A. Hochwagen, 2010 A Mec1- and PP4-dependent checkpoint couples centromere pairing to meiotic recombination. Dev Cell 19**:** 599-611.

Farmer, S., E. J. Hong, W. K. Leung, B. Argunhan, Y. Terentyev *et al.*, 2012 Budding yeast Pch2, a widely conserved meiotic protein, is involved in the initiation of meiotic recombination. PLoS One 7**:** e39724.

Garcia, V., S. Gray, R. M. Allison, T. J. Cooper and M. J. Neale, 2015 Tel1(ATM)-mediated interference suppresses clustered meiotic double-strand-break formation. Nature 520**:** 114-118.

Herruzo, E., A. Lago-Maciel, S. Baztan, B. Santos, J. A. Carballo *et al.*, 2021 Pch2 orchestrates the meiotic recombination checkpoint from the cytoplasm. PLoS Genet 17**:** e1009560.

Herruzo, E., D. Ontoso, S. Gonzalez-Arranz, S. Cavero, A. Lechuga *et al.*, 2016 The Pch2 AAA+ ATPase promotes phosphorylation of the Hop1 meiotic checkpoint adaptor in response to synaptonemal complex defects. Nucleic Acids Res 44**:** 7722-7741.

Ho, H. C., and S. M. Burgess, 2011 Pch2 acts through Xrs2 and Tel1/ATM to modulate interhomolog bias and checkpoint function during meiosis. PLoS Genet 7**:** e1002351.

Hoffmann, R., S. Jung, M. Ehrmann and H. W. Hofer, 1994 The Saccharomyces cerevisiae gene PPH3 encodes a protein phosphatase with properties different from PPX, PP1 and PP2A. Yeast 10**:** 567-578.

Hollingsworth, N. M., and B. Byers, 1989 HOP1: a yeast meiotic pairing gene. Genetics 121**:** 445-462.

Hollingsworth, N. M., L. Goetsch and B. Byers, 1990 The HOP1 gene encodes a meiosis-specific component of yeast chromosomes. Cell 61**:** 73-84.

738 Hustedt, N., A. Seeber, R. Sack, M. Tsai-Pflugfelder, B. Bhullar *et al.*, 2015 Yeast PP4
739 interacts with ATR homolog Ddc2-Mec1 and regulates checkpoint signaling.
740 Mol Cell 57**:** 273-289.
741 Iwasaki, D., K. Hayashihara, H. Shima, M. Higashide, M. Terasawa *et al.*, 2016 The
742 MRX Complex Ensures NHEJ Fidelity through Multiple Pathways Including
743 Xrs2-FHA-Dependent Tel1 Activation. PLoS Genet 12**:** e1005942.
744 Joshi, N., M. S. Brown, D. K. Bishop and G. V. Borner, 2015 Gradual implementation
745 of the meiotic recombination program via checkpoint pathways controlled by
746 global DSB levels. Mol Cell 57**:** 797-811.
747 Kato, R., and H. Ogawa, 1994 An essential gene, ESR1, is required for mitotic cell
748 growth, DNA repair and meiotic recombination in Saccharomyces cerevisiae.
749 Nucleic Acids Res 22**:** 3104-3112.
750 Keeney, S., 2001 Mechanism and control of meiotic recombination initiation. Curr Top
751 Dev Biol 52**:** 1-53.
752 Keogh, M. C., J. A. Kim, M. Downey, J. Fillingham, D. Chowdhury *et al.*, 2006 A
753 phosphatase complex that dephosphorylates gammaH2AX regulates DNA
754 damage checkpoint recovery. Nature 439**:** 497-501.
755 Kim, K. P., B. M. Weiner, L. Zhang, A. Jordan, J. Dekker *et al.*, 2010 Sister cohesion
756 and structural axis components mediate homolog bias of meiotic recombination.
757 Cell 143**:** 924-937.
758 Klein, F., P. Mahr, M. Galova, S. B. Buonomo, C. Michaelis *et al.*, 1999 A central role
759 for cohesins in sister chromatid cohesion, formation of axial elements, and
760 recombination during yeast meiosis. Cell 98**:** 91-103.
761 Kugou, K., T. Fukuda, S. Yamada, M. Ito, H. Sasanuma *et al.*, 2009 Rec8 guides
762 canonical Spo11 distribution along yeast meiotic chromosomes. Mol Biol Cell
763 20**:** 3064-3076.
764 Lai, Y. J., F. M. Lin, M. J. Chuang, H. J. Shen and T. F. Wang, 2011 Genetic
765 requirements and meiotic function of phosphorylation of the yeast axial element
766 protein Red1. Mol Cell Biol 31**:** 912-923.
767 Lee, B. H., and A. Amon, 2003 Role of Polo-like kinase CDC5 in programming meiosis
768 I chromosome segregation. Science 300**:** 482-486.
769 Lo, Y. H., C. N. Chuang and T. F. Wang, 2014 Pch2 prevents Mec1/Tel1-mediated
770 Hop1 phosphorylation occurring independently of Red1 in budding yeast
771 meiosis. PLoS One 9**:** e85687.

772 Niu, H., L. Wan, B. Baumgartner, D. Schaefer, J. Loidl *et al.*, 2005 Partner choice
773 during meiosis is regulated by Hop1-promoted dimerization of Mek1. Mol Biol
774 Cell 16**:** 5804-5818.
775 Novak, J. E., P. B. Ross-Macdonald and G. S. Roeder, 2001 The budding yeast Msh4
776 protein functions in chromosome synapsis and the regulation of crossover
777 distribution. Genetics 158**:** 1013-1025.
778 O'Neill, B. M., S. J. Szyjka, E. T. Lis, A. O. Bailey, J. R. Yates, 3rd *et al.*, 2007 Pph3-
779 Psy2 is a phosphatase complex required for Rad53 dephosphorylation and
780 replication fork restart during recovery from DNA damage. Proc Natl Acad Sci
781 U S A 104**:** 9290-9295.
782 Panizza, S., M. A. Mendoza, M. Berlinger, L. Huang, A. Nicolas *et al.*, 2011 Spo11-
783 accessory proteins link double-strand break sites to the chromosome axis in
784 early meiotic recombination. Cell 146**:** 372-383.
785 Penedos, A., A. L. Johnson, E. Strong, A. S. Goldman, J. A. Carballo *et al.*, 2015
786 Essential and Checkpoint Functions of Budding Yeast ATM and ATR during
787 Meiotic Prophase Are Facilitated by Differential Phosphorylation of a Meiotic
788 Adaptor Protein, Hop1. PLoS One 10**:** e0134297.
789 Raina, V. B., and G. Vader, 2020 Homeostatic Control of Meiotic Prophase Checkpoint
790 Function by Pch2 and Hop1. Curr Biol 30**:** 4413-4424 e4415.
791 Rao, H. B. D. P., T. Sato, K. Challa, M. Shinohara and A. Shinohara, 2020
792 Phosphorylation of luminal region of the SUN-domain protein Mps3 promotes
793 nuclear envelope localization during meiosis. bioRxiv**:** 2020.2009.2015.297762.
794 Ritchie, K. B., J. C. Mallory and T. D. Petes, 1999 Interactions of TLC1 (which encodes
795 the RNA subunit of telomerase), TEL1, and MEC1 in regulating telomere length
796 in the yeast Saccharomyces cerevisiae. Mol Cell Biol 19**:** 6065-6075.
797 Rockmill, B., and G. S. Roeder, 1988 RED1: a yeast gene required for the segregation
798 of chromosomes during the reductional division of meiosis. Proc Natl Acad Sci
799 U S A 85**:** 6057-6061.
800 San-Segundo, P. A., and G. S. Roeder, 1999 Pch2 links chromatin silencing to meiotic
801 checkpoint control. Cell 97**:** 313-324.
802 Schwacha, A., and N. Kleckner, 1997 Interhomolog bias during meiotic recombination:
803 meiotic functions promote a highly differentiated interhomolog-only pathway.
804 Cell 90**:** 1123-1135.
805 Shi, Y., 2009 Serine/threonine phosphatases: mechanism through structure. Cell 139**:**
806 468-484.

807 Shinohara, A., S. Gasior, T. Ogawa, N. Kleckner and D. K. Bishop, 1997
808 Saccharomyces cerevisiae recA homologues RAD51 and DMC1 have both
809 distinct and overlapping roles in meiotic recombination. Genes Cells 2: 615-629.
810 Shinohara, M., D. K. Bishop and A. Shinohara, 2019 Distinct Functions in Regulation
811 of Meiotic Crossovers for DNA Damage Response Clamp Loader
812 Rad24(Rad17) and Mec1(ATR) Kinase. Genetics 213: 1255-1269.
813 Shinohara, M., S. L. Gasior, D. K. Bishop and A. Shinohara, 2000 Tid1/Rdh54
814 promotes colocalization of rad51 and dmc1 during meiotic recombination. Proc
815 Natl Acad Sci U S A 97: 10814-10819.
816 Shinohara, M., K. Hayashihara, J. T. Grubb, D. K. Bishop and A. Shinohara, 2015 DNA
817 damage response clamp 9-1-1 promotes assembly of ZMM proteins for
818 formation of crossovers and synaptonemal complex. J Cell Sci 128: 1494-1506.
819 Shinohara, M., S. D. Oh, N. Hunter and A. Shinohara, 2008 Crossover assurance and
820 crossover interference are distinctly regulated by the ZMM proteins during yeast
821 meiosis. Nat Genet 40: 299-309.
822 Shinohara, M., K. Sakai, T. Ogawa and A. Shinohara, 2003 The mitotic DNA damage
823 checkpoint proteins Rad17 and Rad24 are required for repair of double-strand
824 breaks during meiosis in yeast. Genetics 164: 855-865.
825 Shinohara, M., and A. Shinohara, 2013 Multiple pathways suppress non-allelic
826 homologous recombination during meiosis in Saccharomyces cerevisiae. PLoS
827 One 8: e63144.
828 Storlazzi, A., L. Xu, A. Schwacha and N. Kleckner, 1996 Synaptonemal complex (SC)
829 component Zip1 plays a role in meiotic recombination independent of SC
830 polymerization along the chromosomes. Proc Natl Acad Sci U S A 93: 9043-
831 9048.
832 Subramanian, V. V., A. J. MacQueen, G. Vader, M. Shinohara, A. Sanchez *et al.*, 2016
833 Chromosome Synapsis Alleviates Mek1-Dependent Suppression of Meiotic
834 DNA Repair. PLoS Biol 14: e1002369.
835 Sun, X., L. Huang, T. E. Markowitz, H. G. Blitzblau, D. Chen *et al.*, 2015 Transcription
836 dynamically patterns the meiotic chromosome-axis interface. Elife 4.
837 Sym, M., J. A. Engebrecht and G. S. Roeder, 1993 ZIP1 is a synaptonemal complex
838 protein required for meiotic chromosome synapsis. Cell 72: 365-378.
839 Tsubouchi, T., and G. S. Roeder, 2005 A synaptonemal complex protein promotes
840 homology-independent centromere coupling. Science 308: 870-873.
841 Villoria, M. T., P. Gutierrez-Escribano, E. Alonso-Rodriguez, F. Ramos, E. Merino *et*
842 *al.*, 2019 PP4 phosphatase cooperates in recombinational DNA repair by

843 enhancing double-strand break end resection. Nucleic Acids Res 47: 10706-
844 10727.
845 Wan, L., C. Zhang, K. M. Shokat and N. M. Hollingsworth, 2006 Chemical inactivation
846 of cdc7 kinase in budding yeast results in a reversible arrest that allows efficient
847 cell synchronization prior to meiotic recombination. Genetics 174: 1767-1774.
848 Weinert, T. A., G. L. Kiser and L. H. Hartwell, 1994 Mitotic checkpoint genes in
849 budding yeast and the dependence of mitosis on DNA replication and repair.
850 Genes Dev 8: 652-665.
851 West, A. M. V., E. A. Komives and K. D. Corbett, 2018 Conformational dynamics of
852 the Hop1 HORMA domain reveal a common mechanism with the spindle
853 checkpoint protein Mad2. Nucleic Acids Res 46: 279-292.
854 Zhang, L., K. P. Kim, N. E. Kleckner and A. Storlazzi, 2011 Meiotic double-strand
855 breaks occur once per pair of (sister) chromatids and, via Mec1/ATR and
856 Tel1/ATM, once per quartet of chromatids. Proc Natl Acad Sci U S A 108:
857 20036-20041.
858 Zhao, X., E. G. Muller and R. Rothstein, 1998 A suppressor of two essential checkpoint
859 genes identifies a novel protein that negatively affects dNTP pools. Mol Cell 2:
860 329-340.
861 Zhu, Z., S. Mori, H. Oshiumi, K. Matsuzaki, M. Shinohara *et al.*, 2010 Cyclin-
862 dependent kinase promotes formation of the synaptonemal complex in yeast
863 meiosis. Genes Cells 15: 1036-1050.
864
865

866 **Figure legends**

867

868 **Figure1. PP4 dephosphorylation activity is required for proper meiotic**

869 **recombination.**

870 (A) Schematic of the functional domain structure of yeast Pph3 (*sc*Pph3) protein.

871 Amino acid sequences contributing to phosphate binding and metal coordination

872 are shown in pale blue and red, respectively. The position of the *pph3-H112N*

873 and the substitution of histidine 112 with asparagine is shown.

874 (B) Localization of Psy2-13Myc was assessed in *PPH3* (MSY6198/6190) and the

875 *pph3-H112N* (MSY6242/6244) background was assessed via immunostaining

876 with anti-Myc antibody (green). Representative images at 6h in meiosis are

877 shown**.** Scale bar indicates 2 μm.

878 (C) Schematics of the *HIS4-LEU2* recombination hotspot. Diagnostic P: *Pst*I, X: *Xho*I,

879 B: *Bam*HI and M: *Mlu*I restriction sites are shown. The size of meiotic DSBs (DSB

880 I, DSB II), and parental (Pa), and heteroduplexes (HDs) that are associated with

881 COs (HD2 and HD3) or NCOs (HD1 and HD4), Parental (Pa1 and Pa2), and the

882 positions of detectable probes 291 and 155 are shown.

883 (D) Representative Southern blotting of DSB detection in wild type (black,

884 NKY1303/1543), *pph3*Δ (red, MSY5632/MSY5634), *pph3-H112N* (blue,

885 MSY6219/6220), p*CLB2-MEC1 tel1*Δ (purple, MSY5544/5546), and p*CLB2-*

886 *MEC1 tel1*Δ *pph3*Δ (orange, MSY5760/5762) using probe 291. The graph shows

887 the mean and standard error of the quantified DSB I signals from more than three

888 reperated trials.

889 (E) Representative Southern blotting of HD-associated COs and NCOs formed at the

890 *HIS4-LEU2* hotspot using probe155. The upper graph shows the mean and
891 standard error of the quantified HD-associated COs (HD2 and HD3). The lower
892 graph shows the mean and standard error of the quantified HD-associated NCOs
893 (HD1 and HD4) of wild type, *pph3*Δ, and *pph3-H112N.*
894 (F) Representative immunostaining images of Rad51 (green) at 3 h on meiotic
895 nuclear spreads in wild type (NKY1303/1543), *pph3*Δ (MSY5632/MSY5634), and
896 *pph3-H112N* (MSY6219/6220). Scale bar indicates 2 μm. The dot plot graph
897 shows the distribution of the number of Rad51 foci in each Rad51 focus positive
898 nucleus at the indicated time points in wild type (black, NKY1303/1543), *pph3*Δ
899 (red, MSY5632/MSY5634), and *pph3-H112N* (blue, MSY6219/6220). The data
900 are presented as the medians and 95% confidence interval. Asterisks indicate
901 statistically significant differences between the indicated strains determined using
902 the Mann-Whitney U-test (* $P<0.05$, ** $P<0.01$, **** $P<0.0001$) using Prism9
903 software.
904
905 **Figure 2. Hop1 assembly is delayed in the *pph3* mutant in early prophase-I.**
906 (A) Graphical depiction of the kinetics of Hop1 focus (upper) assembly on meiotic
907 nuclear spreads in the indicated strains, wild type (black, NKY1303/1543), *pph3*Δ
908 (red, MSY5632/MSY5634), *pph3-H112N* (blue, MSY6219/6220), p*CLB2-MEC1*
909 *tel1*Δ (purple, MSY5544/5546), p*CLB2-MEC1 tel1*Δ *pph3*Δ (orange,
910 MSY5760/5762), *spo11-Y135F* (green, MSY4139/4141), and *spo11-Y135F*
911 *pph3-H112N* (pale blue, MSY6568/6570). From the above graph, 2 h and 3 h
912 data were extracted and re-presented as a box plot with statistical analysis.
913 Whiskers show the median and interquartile range. More than 100 cells ere

914 analyzed in each time point. Statistically significant differences were determined
915 using Student's t-test (**$P < 0.001$, *** $P < 0.0005$, **** $P < 0.0001$) using Prism9
916 software.
917 (B) Representative cytological immunostaining images of Hop1 (green) and Hop1-
918 pT318 (red) on meiotic nuclear spreads at 3 h in each strain shown in Figure 2A.
919 Scale bar indicates 2 μm.
920 (C) Graphical depiction of the kinetics of Hop1-pT318 focus (left) assembly on
921 meiotic nuclear spreads in the indicated strains. The dot plot graph (right) shows
922 the distributions of the number of Hop1-pT318 foci in each Hop1-pT318 focus
923 positive nucleus at 4 and 5 h in wild type, *pph3*Δ, *pph3-H112N*, p*CLB2-MEC1*
924 *tel1*Δ, and p*CLB2-MEC1 tel1*Δ *pph3*Δ. The data are presented as the medians
925 and 95% confidence interval. N denotes number analyzed. Statistically significant
926 differences were determined using Mann-Whitney's U-test (**** $P < 0.0001$) using
927 Prism9 software.
928 (D) Representative western blot images of phosphorylation of histone H2A (γH2A,
929 red) and α-tubulin (green) at the indicated time point during meiosis (upper panel).
930 Hop1 (green, top), phosphorylation of Hop1 at T318 (Hop1-pT318, red, middle),
931 merged images of Hop1 and Hop1-pT318, and α-tubulin (bottom) at the indicated
932 time points during meiosis. M denotes molecular weight markers.
933
934 **Figure 3. Rec8 appeared in normal timing in the *pph3* mutant in early prophase I.**
935 (A) Representative cytological immunostaining images of Rec8 (green) and Red1
936 (red) on meiotic nuclear spreads at 3 h in wild type (NKY1303/1543), *pph3*Δ
937 (MSY5632/MSY5634), *pph3-H112N* (MSY6219/6220). wild type

938 (NKY1303/1543), *pch2*Δ (MSY6446/6448), *pph3*Δ (MSY5632/MSY5634), and
939 *pph3*Δ *pch2*Δ (MSY6417/6419)
940 (B) Left graphs show the kinetics of Red1 (upper) and Rec8 (lower) focus assembly
941 on meiotic nuclear spreads in the indicated strains, wild type (black,
942 NKY1303/1543), *pph3*Δ (red, MSY5632/MSY5634), and *pph3-H112N* (blue,
943 MSY6219/6220). More than 100 cells were analyzed at each time point. Error
944 bars show the mean ± standard deviation of more than three trial repetitions.
945 Right box whiskers plots show distributions of frequencies (%) of nuclei positive
946 for Red1 (upper) or Rec8 (lower) at 2 or 3 h from the data sets shown in the left
947 graphs. Whiskers show the median and interquartile range. Statistically
948 significant differences were determined using Welch's t-test (* $P < 0.05$, ** $P <$
949 0.01) using Prism9 software.
950 (C) Representative western blot images of Rec8 (upper) and Red1 (lower), with α-
951 tubulin images as internal controls, at the indicated meiotic time points. M
952 denotes molecular weight markers. Asterisks indicate non-specific protein signals.
953 (D) Graphical depiction of the kinetics of Red1 focus assembly on meiotic nuclear
954 spreads in the *spo11-Y135F* (black, MSY4139/4141) and *spo11-Y135F pph3-*
955 *H112N* (blue, MSY6568/6570). More than 100 cells were analyzed in each time
956 point. Error bars show the mean ± standard deviation of more than three repeated
957 trials.
958
959 **Figure 4. PP4 interacts with Hop1 during meiosis.**
960 (A) Immunoprecipitation (IP) analysis of Psy2-13Myc from *PPH3* (non-tag,
961 NKY1303/1543) and *PPH3* (*PSY2-13MYC*, MSY6188/6190) cells at the indicated

962 time points during meiosis. Whole cell extracts (WCEs) and IP products were
963 probed with anti-Myc, anti-Hop1, anti-Red1 and anti-Rec8 antibodies. Small
964 arrows show the modified products.

965 (B) Tetrad analysis of spore viability in wild type (NKY1303/1543), *pph3*Δ
966 (MSY5632/MSY5634), *pch2*Δ (MSY6446/6448), and *pph3*Δ *pch2*Δ
967 (MSY6417/6419). The graphs show the fraction of tetrads containing 0-, 1-, 2-,
968 3- and 4-viable spores. The overall spore viability is shown in parentheses. n:
969 number of asci analyzed.

970 (C) Graphical depiction of the kinetics of Hop1 (left) and Hop1-pT318 (right) focus
971 assembly on meiotic nuclear spreads in the indicated strains: wild type (black,
972 NKY1303/1543), *pch2*Δ (gray, MSY6446/6448), *pph3*Δ (red,
973 MSY5632/MSY5634), and *pph3*Δ *pch2*Δ (orange, MSY6417/6419). More than
974 100 cells were analyzed per measured time point. Error bars show the mean ±
975 standard deviation of more than three repeated trials.

976 (D) Representative cytological immunostaining images of Hop1 (green) and Hop1-
977 pT318 (red) on meiotic nuclear spreads at 3 h (left panel) and 6 h (right panel) in
978 wild type (NKY1303/1543), *pch2*Δ (MSY6446/6448), *pph3*Δ
979 (MSY5632/MSY5634), and *pph3*Δ *pch2*Δ (MSY6417/6419). Arrowheads show
980 unsynapsed regions. Scale bar indicates 2 μm.

981

982 **Figure 5. *pch2*Δ does not completely suppress the defect in Hop1 assembly**
983 **of *pph3*Δ.**

984 (A) Zip1 and Hop1 elongation was analyzed in wild type (NKY1303/1543), *pch2*Δ
985 (MSY6446/6448), *pph3*Δ (MSY5632/MSY5634), and *pph3*Δ *pch2*Δ

986 (MSY6417/6419) via immunostaining at each time point. The graphs show the
987 percentages of each class of Zip1 morphologies; linear (dark gray, pachytene),
988 partial (pale gray, zygotene), and dotty (black, leptotene). Error bars show the
989 mean ± standard deviation of more than three trials. More than 100 cells at each
990 time point were analyzed.

991 (B) Representative cytological immunostaining images of Hop1 (green) and Zip1
992 (red) on pachytene-phase nuclear spreads at 4 h in wild type (NKY1303/1543),
993 and 6 h in the *pch2*Δ (MSY6446/6448), *pph3*Δ (MSY5632/MSY5634), and *pph3*Δ
994 *pch2*Δ (MSY6417/6419). Scale bar indicates 2 μm.

995 (C) The dot plot graph of the distribution of the number of linearized Hop1 signals in
996 each pachytene stage nucleus in *pch2*Δ (N = 112) and *pph3*Δ *pch2*Δ (N = 109)
997 at 6 h during meiosis from three independent trials. Error bars show the mean
998 with 95% confidence interval. Statistically significant differences between the
999 *pch2*Δ and *pph3*Δ *pch2*Δ were determined using the Mann-Whitney U-test (****
1000 $P < 0.0001$) using Prism9 software.

1001 (D) The dot plot graph of the distribution of lengths of linearized Hop1 signal of
1002 pachytene stage nucleus in *pch2*Δ (gray, N = 718) and *pph3*Δ *pch2*Δ (orange, N
1003 = 780) at 6 h in meiosis from three independent trials. Error bars show the mean
1004 with 95% confidence interval. Statistically significant differences between the
1005 *pch2*Δ and *pph3*Δ *pch2*Δ were determined using the Mann-Whitney U-test (ns;
1006 not significant) using Prism9 software.

1007 (E) Representative cytological immunostaining images of Rec8 (green) and Red1
1008 (red) on pachytene-stage nuclear spreads in wild type (3 h, NKY1303/1543),
1009 *pch2*Δ (6 h, MSY6446/6448), *pph3*Δ (6 h, MSY5632/MSY5634), and *pph3*Δ

1010 *pch2*Δ (6 h, MSY6417/6419). Scale bar indicates 2 μm.

1011 (F) Representative western blot images of Hop1 (green) as well as phosphorylation
1012 of Hop1 at pT318 (Hop1-pT318, red) and α-tubulin (bottom) at the indicated time
1013 points during meiosis. M denotes molecular weight markers.

1014 (G) Meiosis progression in wild type (black, NKY1303/1543), *pch2*Δ (gray,
1015 MSY6446/6448), *pph3*Δ (red, MSY5632/MSY5634), and *pph3*Δ *pch2*Δ (orange,
1016 MSY6417/6419) mutants are shown. Frequencies of nuclei with more than two
1017 DAPI-staining bodies at each time point are plotted. More than 100 cells were
1018 analyzed at each time point. Error bars show the means and standard deviation
1019 of two independent trials.

1020

1021 **Figure 6. Model for PP4 involvement in Hop1 recruitment onto meiotic**
1022 **chromatin.**

1023 PP4 plays multiple roles during meiotic prophase. First, independent of the
1024 introduction of meiotic DSBs and the function of Mec1/Tel1 activated by them,
1025 PP4 promotes Hop1 recruitment in the early phase of meiotic prophase. Until the
1026 onset of chromatin loading, Hop1 exists in an inactive form that may prevent miosis
1027 progression. After meiotic DSB formation, Hop1 is phosphorylated at the DSB site
1028 by Tel1/Mec1, and PP4 is involved in dephosphorylation of the phosphorylated
1029 Hop1. Meiotic recombination promotes homolog synapsis by exchanging Hop1 to
1030 Zip1 through the function of AAA+ Pch2 function.

1031

1032 **Supplemental Figure 1. Supplemental data for Figure 1.**

1033 (A) Representative western blot images of Hop1 (green, top), phosphorylation of

1034 Hop1 at T318 (Hop1-pT318, red, middle), merged images of Hop1 and Hop1-
1035 pT318, and phosphorylation of histone H2A (γH2A, red, bottom) at the indicated
1036 time point during meiosis in *mec1*Δ *sml1*Δ (MSY3643/3644), *mec1*Δ *sml1*Δ *pph3-*
1037 *H112N* (MSY6560/6565), *pCLB2-MEC1* (MSY6551/6552), and *pCLB2-MEC1*
1038 *pph3-H112N* (MSY6574/6576). M denotes molecular weight markers.
1039 (B) Spore viability and the distribution of 4-, 3-, 2-, 1-, and 0-viable spores in wild type
1040 (MSY833/831), *pCLB2-MEC1* (MSY6551/6552), *mec1*Δ *sml1*Δ (MSY3643/3644),
1041 *mec1*-1 *sml1X* (MSY398/399), and *mec1-kd sml1*Δ (MSY4413/4415). n: number
1042 of asci analyzed.
1043 (C) The graph of the kinetics of Rad51 focus assembly on meiotic nuclear spreads
1044 in wild type (black, NKY1303/1543), *pph3*Δ (red, MSY5632/MSY5634), and
1045 *pph3-H112N* (blue, MSY6219/6220). More than 100 cells were analyzed at each
1046 time point. Error bars show the mean ± standard deviation of more than three
1047 trials.
1048
1049 **Supplemental Figure 2. Supplemental data for Figure 2.**
1050 (A) Meiosis progression in wild type (NKY1303/1543), *pph3*Δ (MSY5632/5634),
1051 *pph3-H112N* (MSY6219/6220), *spo11-Y135F*(MSY4139/4141), and *spo11-*
1052 *Y135F pph3-H112N* (MSY6568/6570) mutants. Frequencies of nuclei with more
1053 than two DAPI-stained bodies were plotted. More than 200 cells were analyzed
1054 at each time point.
1055 (B) Graphical depiction of the average number of relative Hop1 protein signals from
1056 western blot at each time point. The numerical values are shown as a percentage
1057 of the peak amount of signal in the wild type. Error bars show the mean and ±

1058 standard deviation of two independent trials.

1059

1060 **Supplemental Figure 3. Supplemental data presentation for Figure 4.**

1061 (A) Whole membrane images of western blot of immunoprecipitates (IP) and whole

1062 cell extracts (WCEs) exhibited in Figure 4A.

1063

1064 **Supplemental Figure 4. Characterization of *hop1-T595L* as a hypomorph allele of**

1065 ***HOP1*.**

1066 (A) Graphical depiction of the kinetics of Hop1, Hop1-pT318, and Red1 focus

1067 assembly on meiotic nuclear spreads in the indicated strains, wild type

1068 (MSY833/831) and *hop1-T595L* (MSY6314/6319) (upper). More than 100 cells

1069 were analyzed at each time point. Error bars show the mean ± standard

1070 deviation of more than three trials. Meiosis progression in wild type

1071 (MSY833/831) and *hop1-T595L* (MSY6314/6319). Frequencies of nuclei with

1072 more than two DAPI-stained bodies were plotted (lower). More than 200 cells

1073 were analyzed at each time point.

1074 (B) Graphical depiction of the kinetics of Hop1 focus assembly on meiotic nuclear

1075 spreads in the indicated strains, *hop1-T595L* (pink, MSY6314/6319), *pph3*Δ

1076 *hop1-T595L* (red, MSY6544/6546), and *pph3-H112N hop1-T595L* (green,

1077 MSY6541/6543). Values of *pph3-H112N* (dark blue) are from the same data

1078 shown in Figure 2A. More than 100 cells were analyzed at each time point.

1079 Error bars show the mean ± standard deviation of more than three trials.

1080 Representative western blot images of Hop1 (green, top), phosphorylation of

1081 Hop1 at T318 (Hop1-pT318, red, middle), and merged images of Hop1 and

1082 Hop1-pT318 at the indicated time point during meiosis in wild type

1083 (MSY833/831), *hop1-T595L* (MSY6314/6319), *pCLB2-MEC1*

1084 (MSY6551/6552), and *pCLB2-MEC1 pph3-H112N* (MSY6574/6576). M

1085 denotes molecular weight markers.

1086

Li *et al* Figure 1

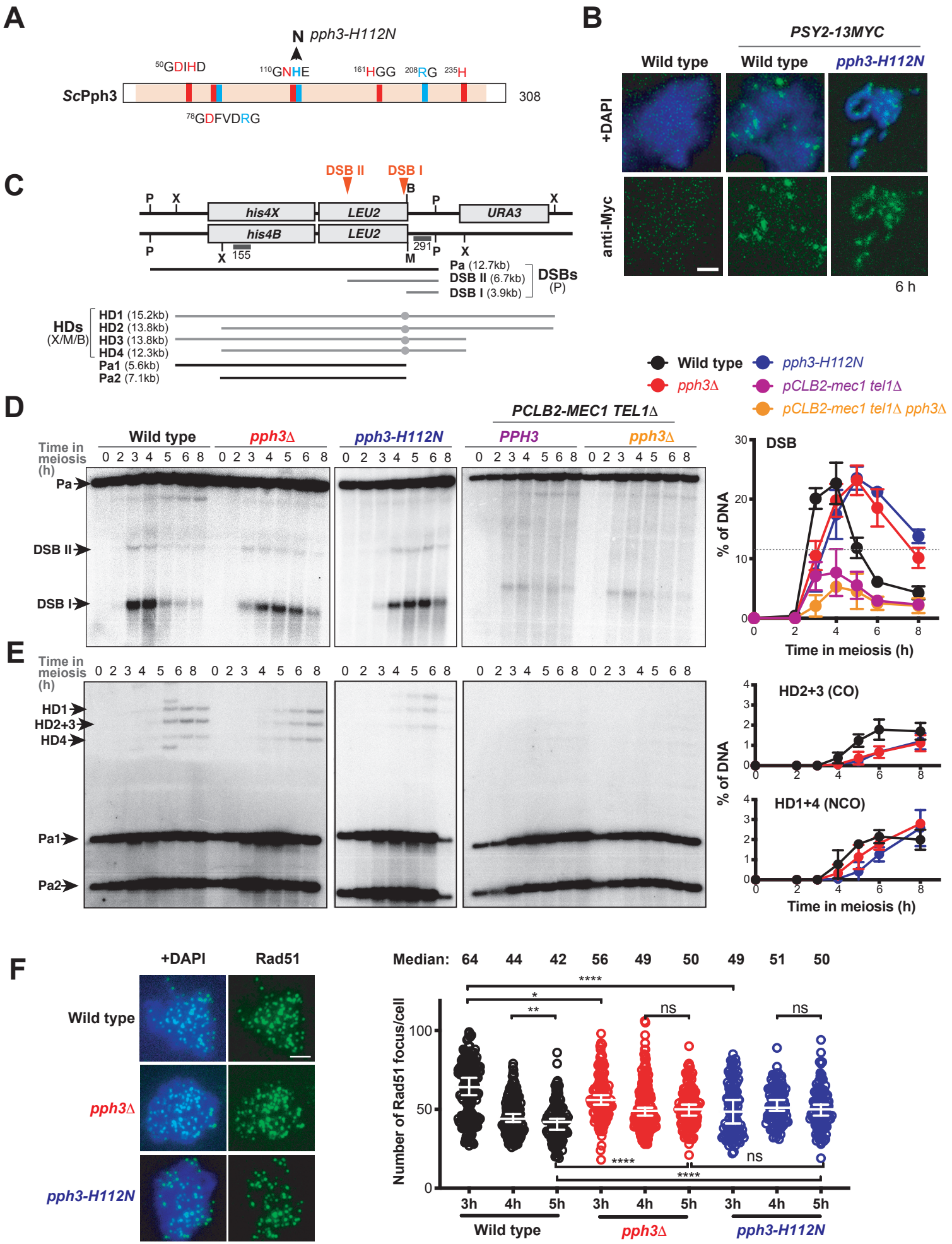

Li *et al* Figure 2

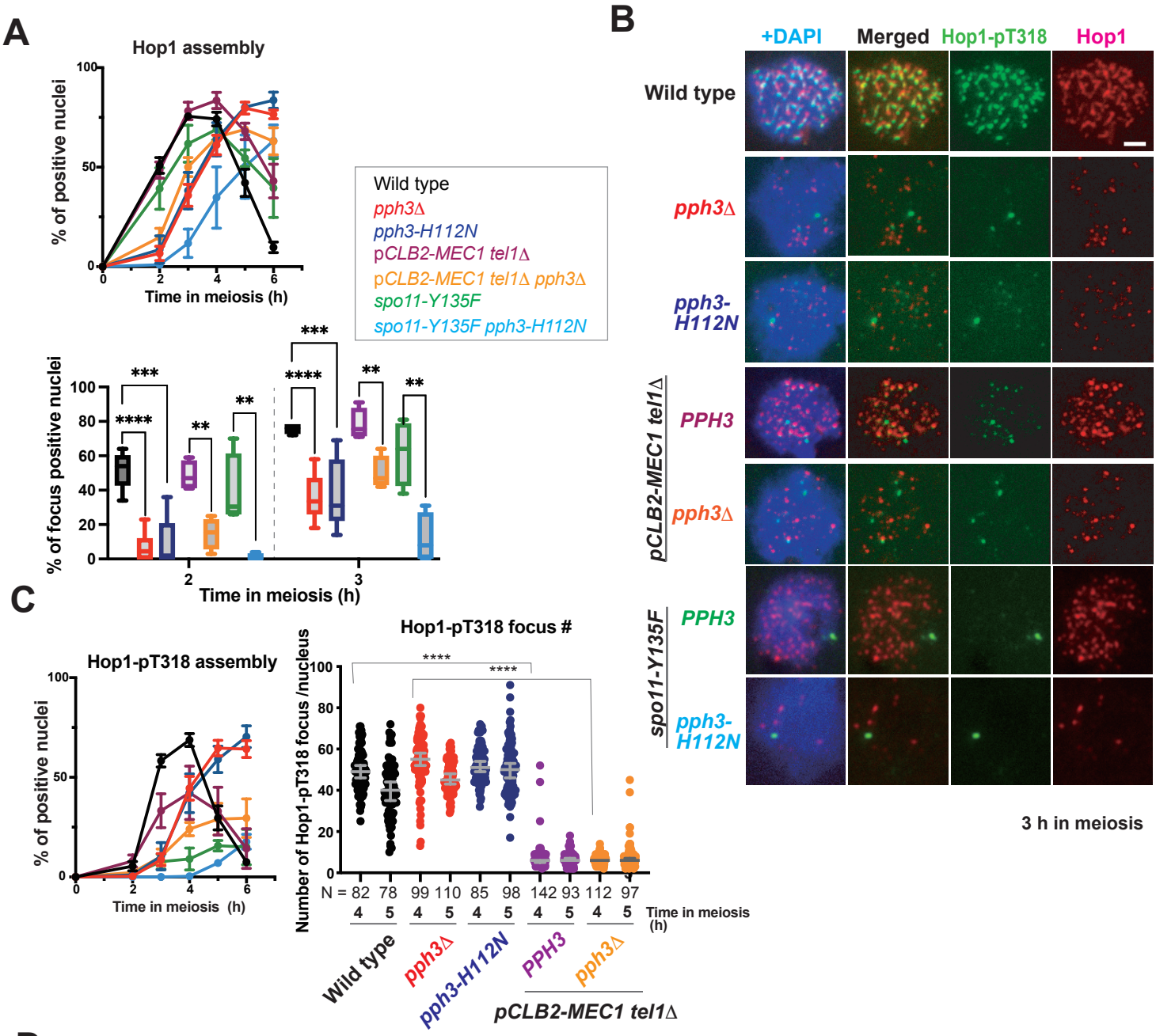

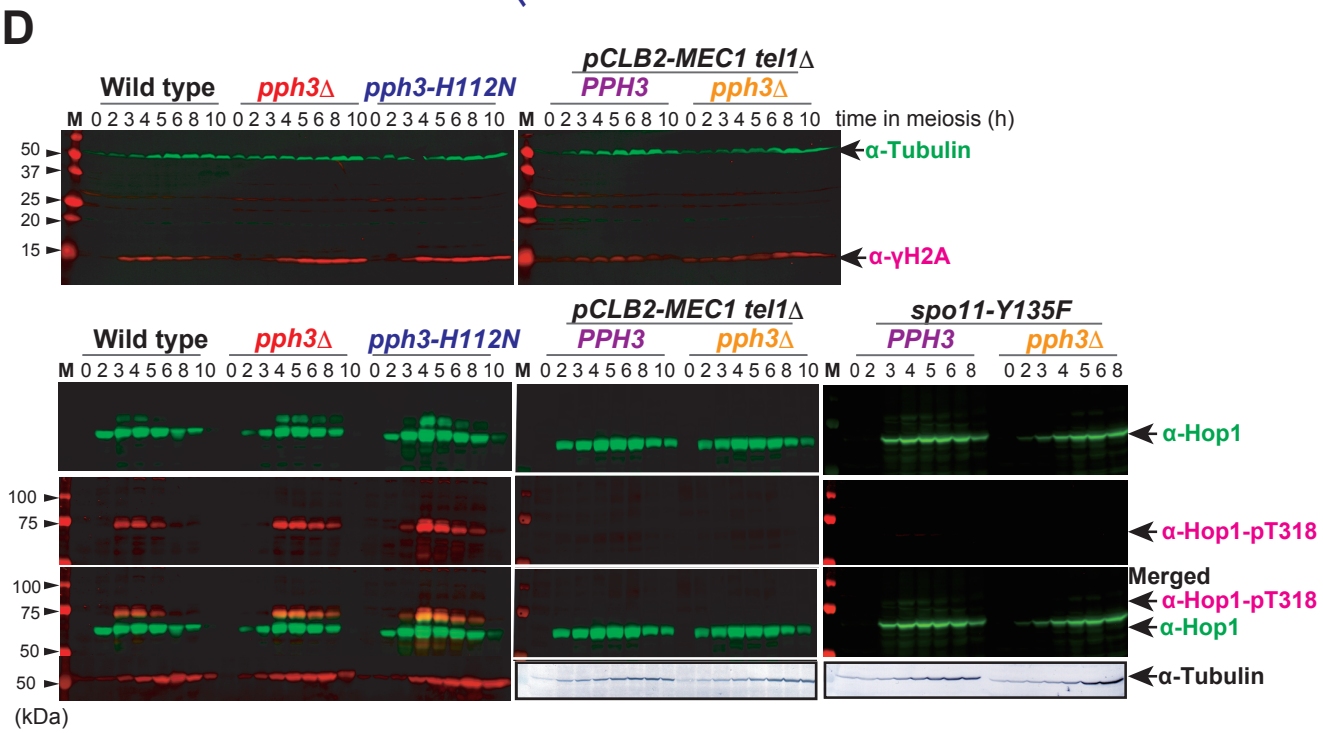

Li *et al* Figure 3

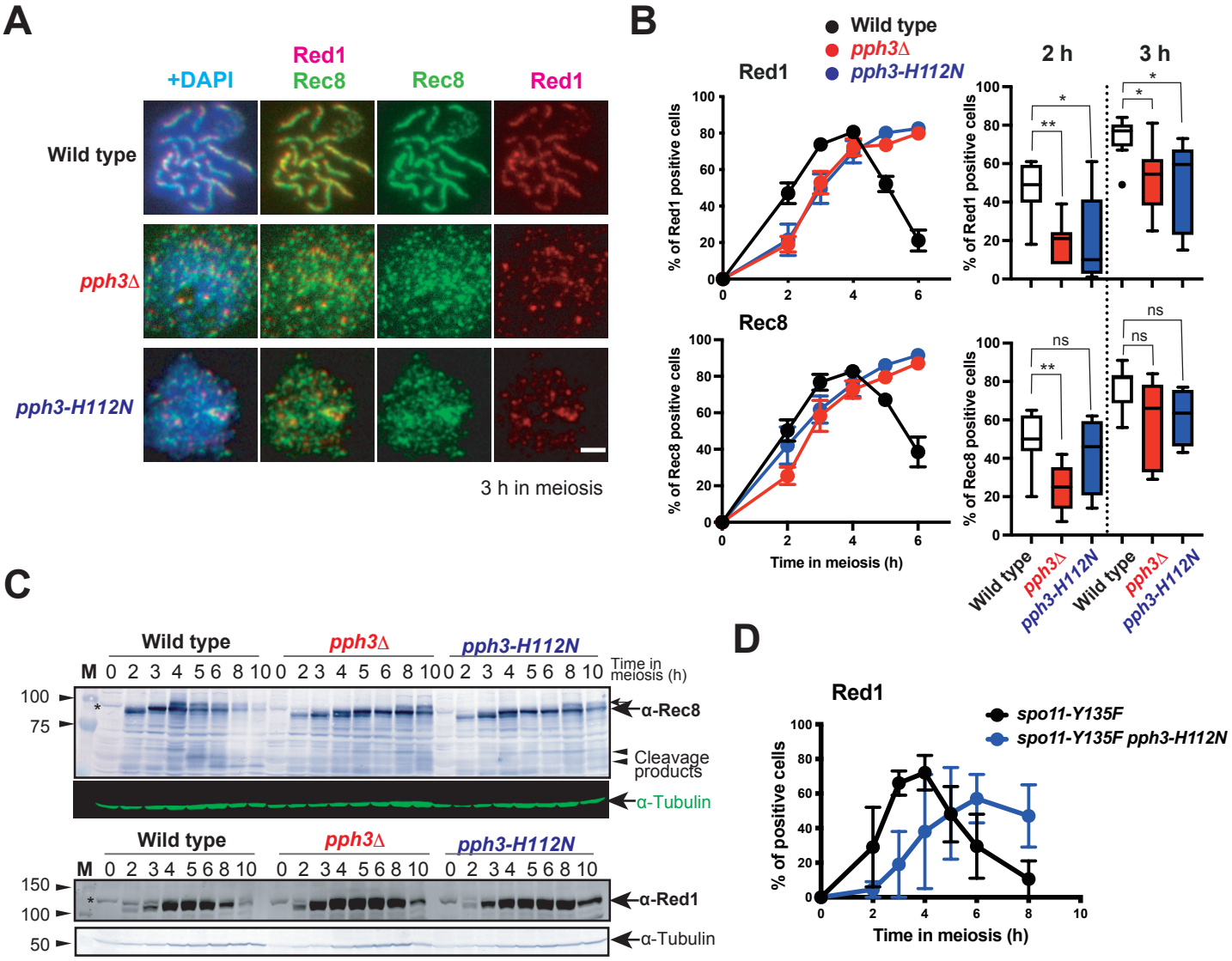

Li *et al* Figure 4

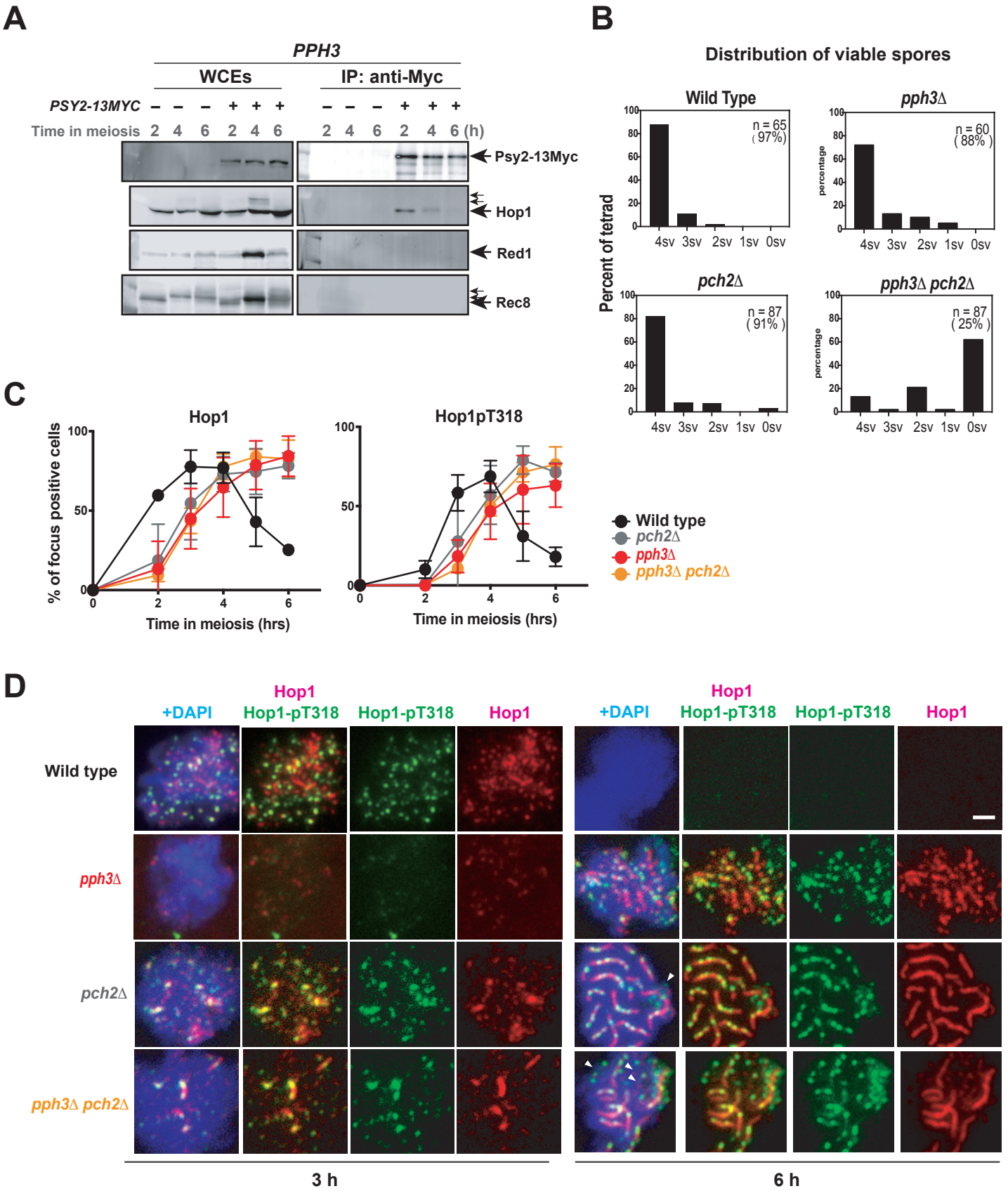

Li *et al* Figure 5

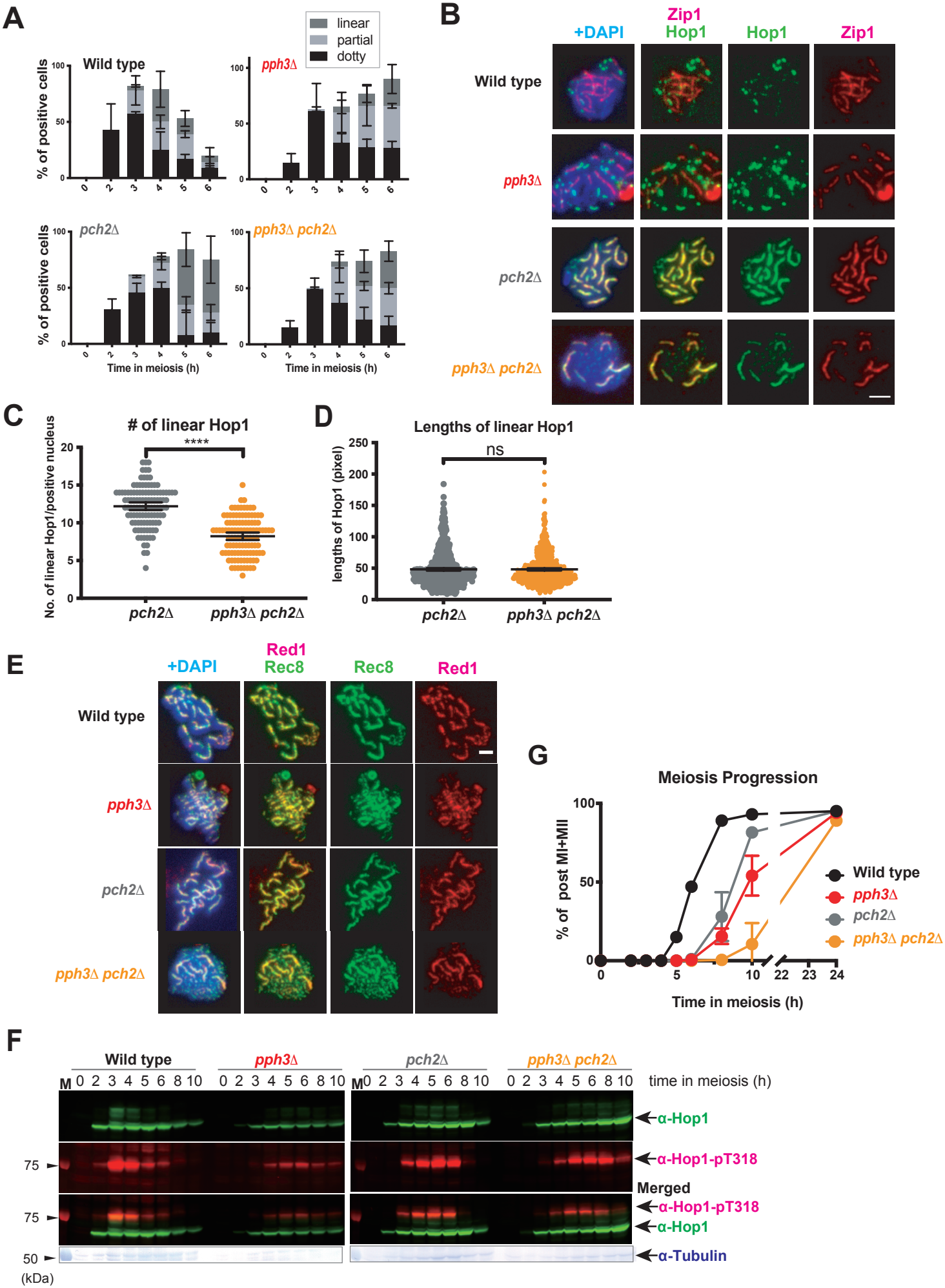

Li *et al*, Figure 6

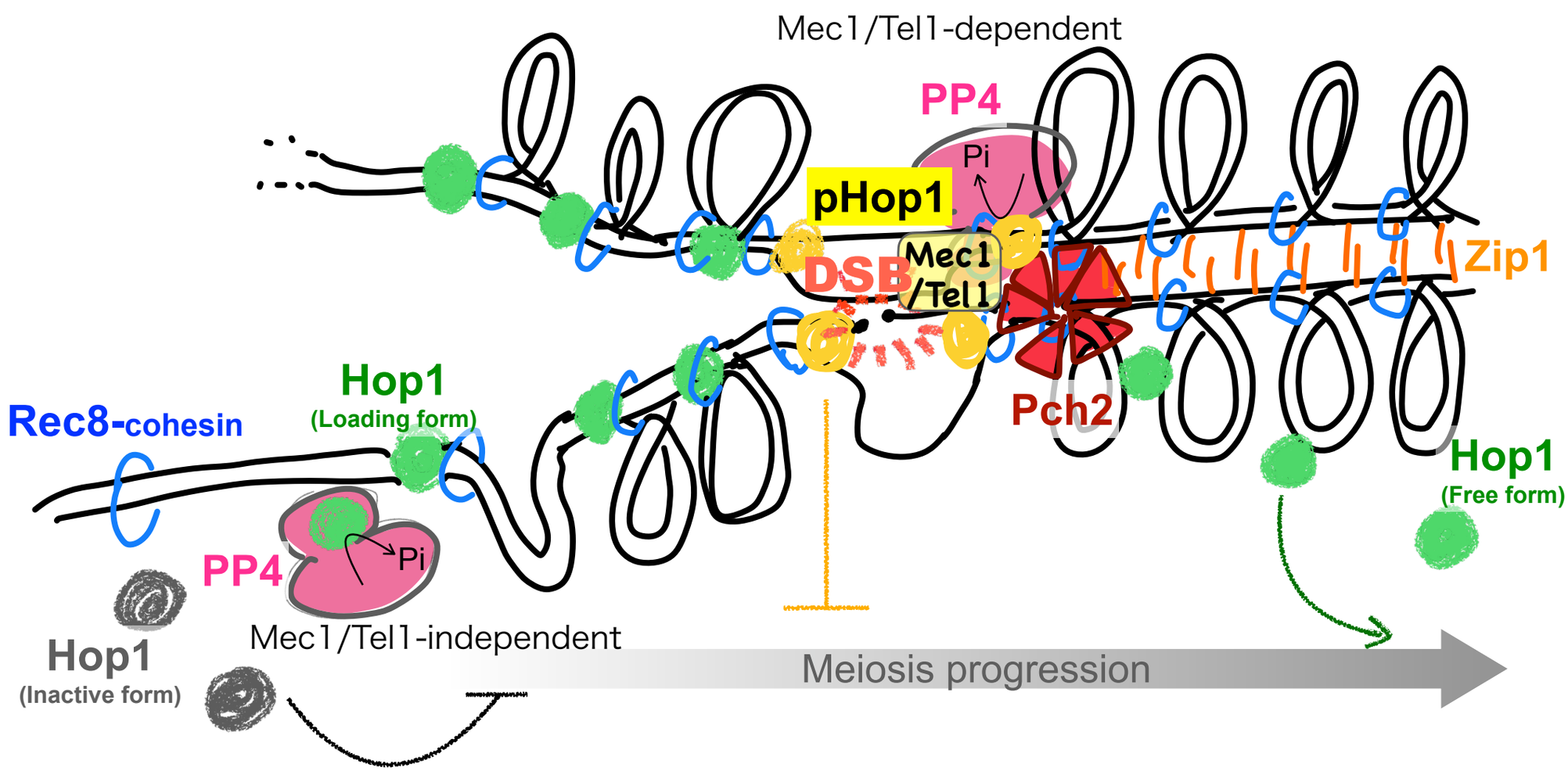

Supplemental Figure 1, Li *et al*

A

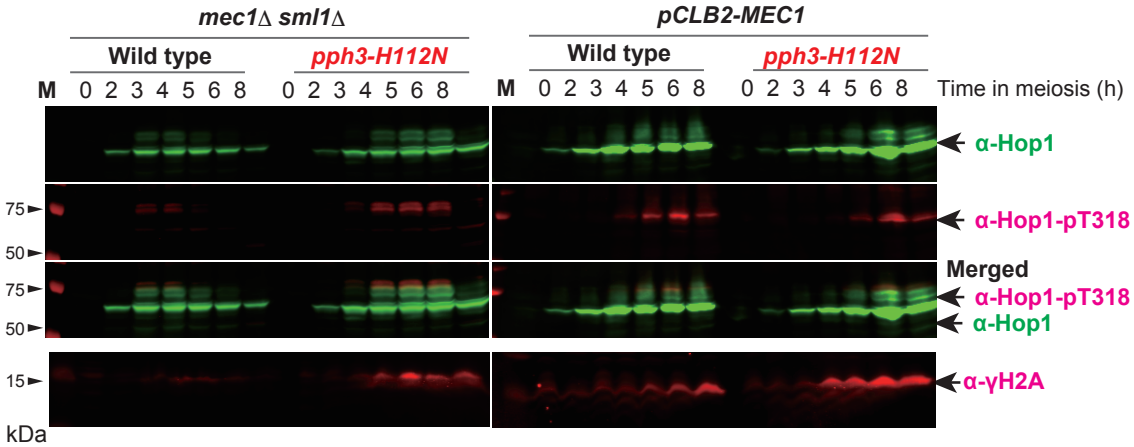

B

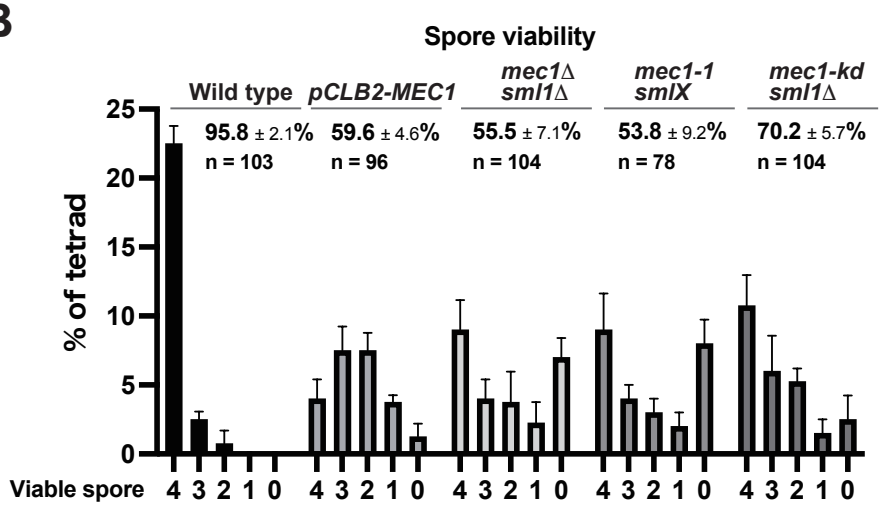

C

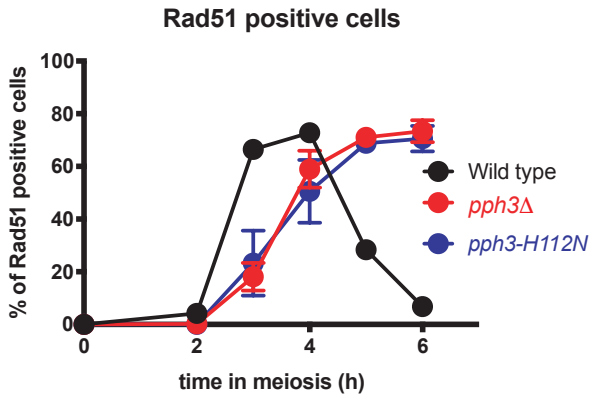

Supplemental Figure 2, Li *et al*

A

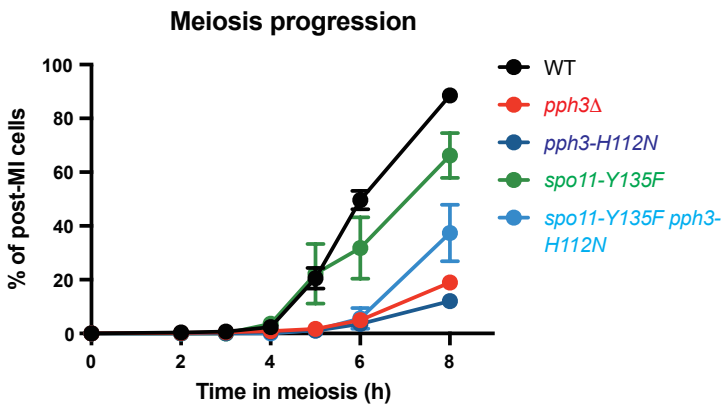

B

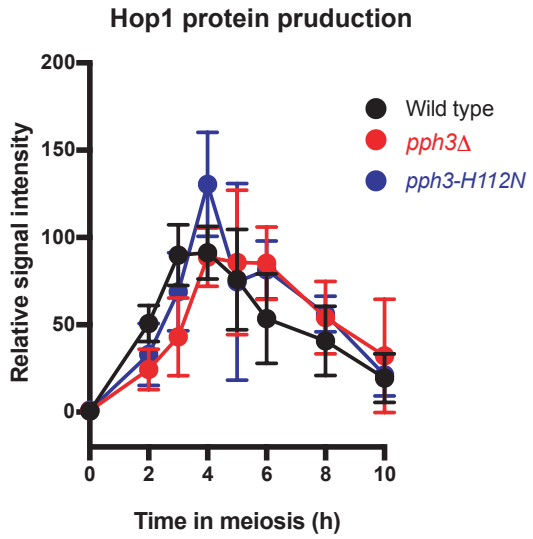

Supplemental Figure 3 Li *et al*

A

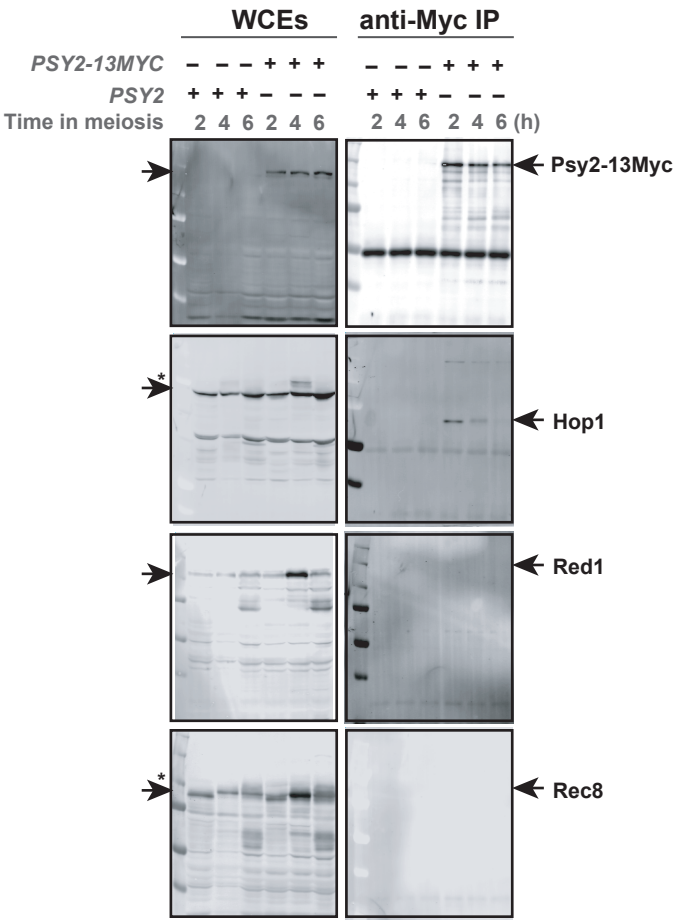

Li *et al* Supplemental Figure 4

A

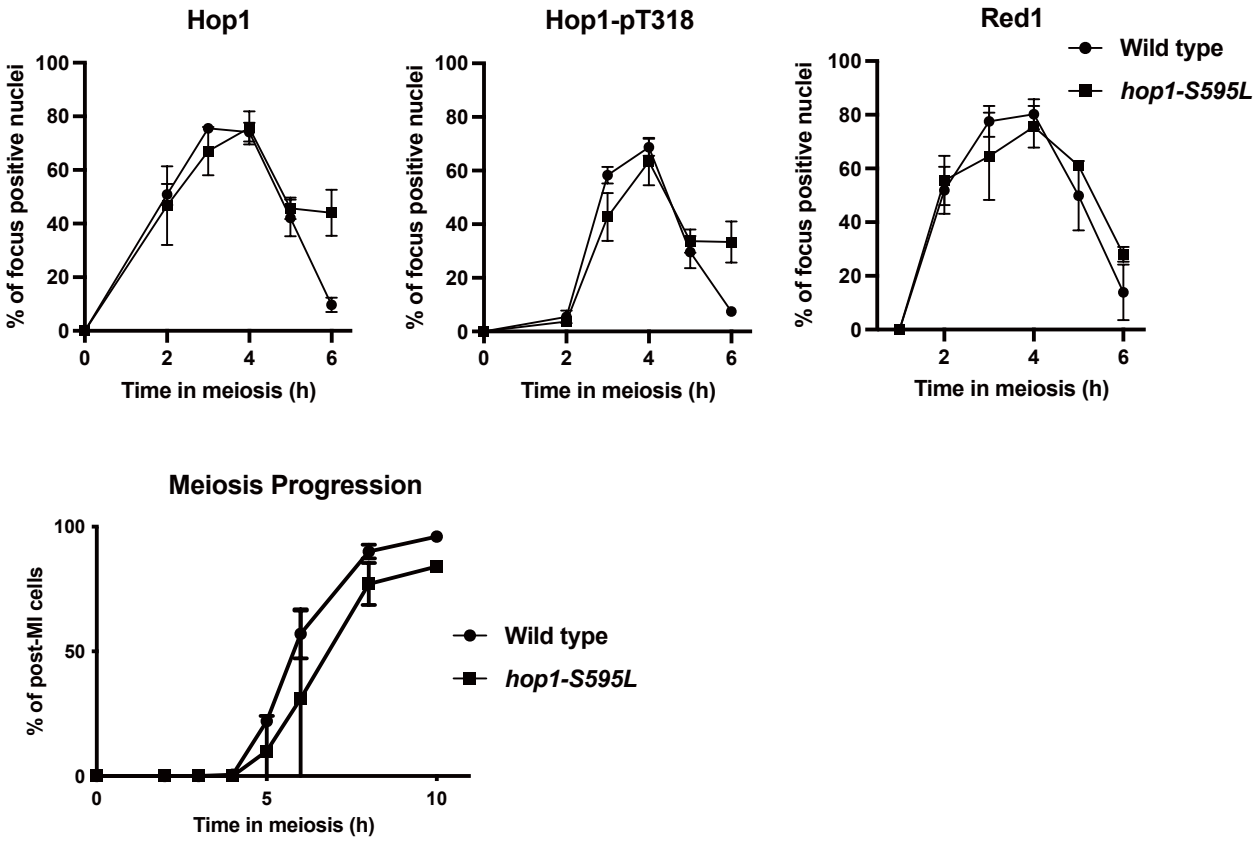

B

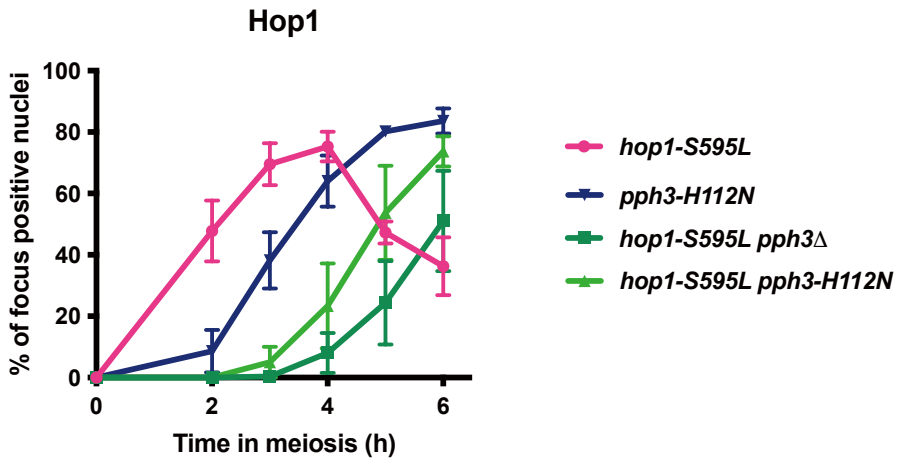

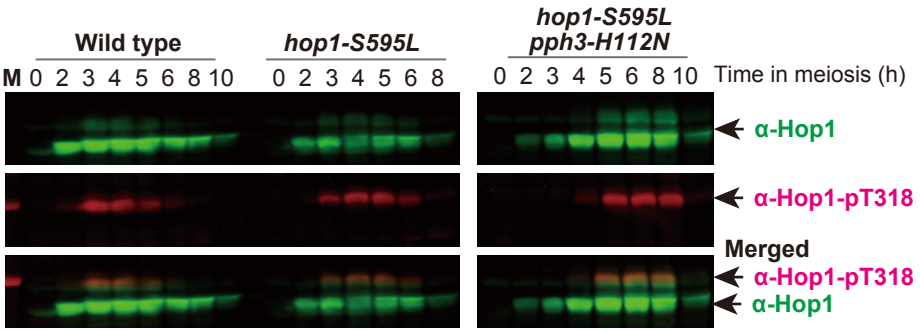

Supplemental Table-1 Strain list

Strain	Genotype	Reference
NKY1303	*MAT*a, *ho::LYS2, lys2, ura3, leu2::hisG, his4B-LEU2(Mlu*I*), arg4-bgl*	(STORLAZZI *et al.* 1996)
NKY1543	*MATa, ho::LYS2, lys2, ura3, leu2::hisG, his4X-LEU2(Bam*HI*)-URA3, arg4-nsp*	(STORLAZZI *et al.* 1996)
MSY831	*MAT*a, *ho::LYS2, lys2, ura3, leu2::hisG, trp1::hisG*	(SHINOHARA *et al.* 2015)
MSY833	*MATa, ho::LYS2, lys2, ura3, leu2::hisG, trp1::hisG*	(SHINOHARA *et al.* 2015)
MSY5632	NKY1303 with *pph3::Hyg*^{R}	This study
MSY5634	NKY1543 with *pph3::Hyg*^{R}	This study
MSY6219	NKY1303 with *pph3-H112N::MluI*	This study
MSY6220	NKY1543 with *pph3-H112N::MluI*	This study
MSY6198	NKY1303 with *PSY2-13MYC::TRP1*	This study
MSY6190	NKY1543 with *PSY2-13MYC::TRP1*	This study
MSY6242	NKY1303 with *PSY2-13MYC::TRP1, pph3-H112N::MluI*	This study
MSY6244	NKY1543 with *PSY2-13MYC::TRP1, pph3-H112N::MluI*	This study
MSY5544	NKY1303 with *pCLB2-MEC1::KANMX, tel1::TRP1*	This study
MSY5546	NKY1543 with *pCLB2-MEC1::KANMX, tel1::TRP1*	This study
MSY5760	NKY1303 with *pCLB2-MEC1::KANMX, tel1::TRP1, pph3::Hyg*^{R}	This study
MSY5762	NKY1543 with *pCLB2-MEC1::KANMX, tel1::TRP1, pph3::Hyg*^{R}	This study
MSY6551	MSY 833 with *pCLB2-MEC1::KANMX*	This study
MSY6552	MSY 831 with *pCLB2-MEC1::KANMX*	This study
MSY6574	MSY 833 with *pph3-H112N*, *pCLB2-MEC1::KANMX*	This study
MSY6576	MSY 831 with *pph3-H112N*, *pCLB2-MEC1::KANMX*	This study
MSY3643	MSY 833 with *mec1::LEU2*, *sml1::KANMX*	This study
MSY3644	MSY 831 with *mec1::LEU2*, *sml1::KANMX*	This study
MSY6560	NKY1303 with *pph3-H112N::MluI, mec1::LEU2*, *sml1::KANMX*	This study
MSY6565	NKY1543 with *pph3-H112N::MluI , mec1::LEU2*, *sml1::KANMX*	This study
MSY4139	MSY833 with *spo11-Y135F*::*KanMX*	This study [a]
MSY4141	MSY831 with *spo11-Y135F*::*KanMX*	This study [a]
MSY6568	MSY833 with *spo11-Y135F*::*KanMX*, *pph3-H112N::Mlu*	This study
MSY6570	MSY831 with *spo11-Y135F*::*KanMX*, *pph3-H112N::Mlu*	This study
MSY6446	NKY1303 with *pch2::TRP1*	This study
MSY6448	NKY1543 with *pch2::TRP1*	This study
MSY6417	NKY1303 with *pph3::Hyg*^{R}, *pch2::TRP1*	This study
MSY6519	NKY1543 with *pph3::Hyg*^{R}, *pch2::TRP1*	This study

MSY398	MSY 833 with *mec1-1*, *smlX*	This study [b]
MSY399	MSY 831 with *mec1-1*, *smlX*	This study [b]
MSY4413	MSY 833 with *mec1-kd (D2224S::XbaI)*, *sml1::KANMX*	This study [c]
MSY4415	MSY 831 with *mec1-kd (D2224S::XbaI)*, *sml1::KANMX*	This study [c]
MSY6314	MSY 833 with *hop1-T595L::SpeI*	This study
MSY6319	MSY 831 with *hop1-T595L::SpeI*	This study
MSY6544	MSY 833 with *pph3::Hyg*^{R}, *hop1-T595L::SpeI*	This study
MSY6546	MSY 831 with *pph3::Hyg*^{R}, *hop1-T595L::SpeI*	This study
MSY6541	MSY 833 with *pph3-H112N::MluI*, *hop1-T595L*::*Spe*I	This study
MSY6543	MSY 831 with *pph3-H112N::MluI*, *hop1-T595L*::*Spe*I	This study

[a] Derivatives of this mutation were already reported in (SHINOHARA *et al.* 2015).

[b] This strain was generated by crossing with the strain which was originally reported in (GRUSHCOW *et al.* 1999).

[c] Derivatives of this mutation were already reported in (SHINOHARA *et al.* 2019).

Grushcow, J. M., T. M. Holzen, K. J. Park, T. Weinert, M. Lichten *et al.*, 1999 Saccharomyces cerevisiae checkpoint genes MEC1, RAD17 and RAD24 are required for normal meiotic recombination partner choice. Genetics 153: 607-620.

Shinohara, M., D. K. Bishop and A. Shinohara, 2019 Distinct Functions in Regulation of Meiotic Crossovers for DNA Damage Response Clamp Loader Rad24(Rad17) and Mec1(ATR) Kinase. Genetics 213: 1255-1269.

Shinohara, M., K. Hayashihara, J. T. Grubb, D. K. Bishop and A. Shinohara, 2015 DNA damage response clamp 9-1-1 promotes assembly of ZMM proteins for formation of crossovers and synaptonemal complex. J Cell Sci 128: 1494-1506.

Storlazzi, A., L. Xu, A. Schwacha and N. Kleckner, 1996 Synaptonemal complex (SC) component Zip1 plays a role in meiotic recombination independent of SC polymerization along the chromosomes. Proc Natl Acad Sci U S A 93: 9043-9048.